Noname manuscript No.
(will be inserted by the editor)

Stochastic and Deterministic Multicloud parameterizations for tropical convection

Yevgeniy Frenkel · Andrew J. Majda · Boualem Khouider

Received: date / Accepted: date

Abstract Despite recent advances in supercomputing, current general circulation models (GCMs) poorly represent the variability associated with organized tropical convection. In a recent study, the authors have shown, in the context of a paradigm two baroclinic mode system, that a stochastic multicloud convective parameterization based on three cloud types (congestus, deep and stratiform) can be used to improve the variability and the dynamical structure of tropical convection. Here, the stochastic multicloud model is modified with a lag type stratiform closure and augmented with an explicit mechanism for congestus detrainment moistening. These modifications

Yevgeniy Frenkel
Department of Mathematics and Center for Atmosphere-Ocean Science, Courant Institute
New York University
251 Mercer Street
New York, NY 10012 USA
Tel.: 212-998-3234
Fax: 212-995-4121
E-mail: frenkel@cims.nyu.edu

Andrew J. Majda
Department of Mathematics and Center for Atmosphere-Ocean Science, Courant Institute
New York University
251 Mercer Street
New York, NY 10012 USA
Tel.: 212-998-3234
Fax: 212-995-3323
E-mail: jonjon@cims.nyu.edu

Boualem Khouider
Department of Mathematics and Statistics
University of Victoria
PO BOX 3045 STN CSC
Victoria, BC
Canada V8W 3P4
Tel. 250-721-7439
Fax. 250-721-8962
E-mail: khouider@math.uvic.ca

improve the representation of intermittent coherent structures such as synoptic and mesoscale convective systems. Moreover, the new stratiform closure allows for increased robustness of the coherent features of the model with respect to the amount of stochastic noise. The simulations with the new closure and a higher amount of stochastic noise result in a Walker type circulation with realistic mean and coherent variability which surpasses results of previous deterministic and stochastic multicloud models in the same parameter regime. Further, deterministic mean field limit equations (DMFLE) for the stochastic multicloud model are considered. Aside from providing a link to the deterministic multicloud parameterization, the DMFLE allow a judicious way of determining the amount of deterministic and stochastic "chaos" in the system. It is shown that with the old stratiform heating closure, the stochastic process accounts for most of the chaotic behavior. The simulations with the new stratiform heating closure exhibit a mixture of stochastic and deterministic chaos. The highly chaotic dynamics in the simulations with congestus detrainment mechanism is due to the strongly nonlinear and numerically stiff deterministic dynamics. In the latter two cases, the DMFLE can be viewed as a "standalone" parameterization, which is capable of capturing some dynamical features of the stochastic parameterization. Furthermore, it is shown that, in spatially extended simulations, the stochastic multicloud model can capture qualitatively two local statistical features of the observations: long and short auto-correlation times of moisture and precipitation, respectively and the approximate power-law in the probability density of precipitation event size for large precipitation events. The latter feature is not reproduced in the column simulations. This fact underscores the importance of gravity waves and large scale moisture convergence.

Keywords Stochastic convective parameterization · Multicloud models · tropical atmospheric dynamics · convectively coupled waves

1 Introduction

Organized convection in the tropics involves a hierarchy of temporal and spatial scales ranging from short lived mesoscale organized squall lines on the order of hundreds of kilometers to intraseasonal oscillations over planetary scales [43,11,54]. Despite the continued research efforts by the climate community, the present coarse resolution GCMs, used for the prediction of weather and climate, poorly represent variability associated with tropical convection [51, 42,50,30,56]. It is believed that the deficiency is due to inadequate treatment of cumulus convection [42,32], which has to be parameterized in the coarse resolution GCMs. Given the importance of the tropics for short-term climate and medium to long range weather prediction, the search for new strategies for parameterizing the unresolved effects of tropical convection has been the focus of researchers during the last few decades.

The problem of adequately addressing the interactions across temporal and spatial scales between the large scale circulation and organized cloud

systems, from individual clouds to large-scale clusters and superclusters to planetary-scale disturbance has been approached from multiple directions. Cloud-resolving models on fine computational grids and high-resolution numerical weather prediction models with improved convective parameterizations have succeeded in representing some aspects of organized convection [4,41]. The other approach has been the development of strategies that directly address the multiscale nature of the problem. Superparameterization (SP) methods [9,7,8,49,34] use a cloud resolving model (CRM) in each column of the large scale GCM to explicitly represent small scale and mesoscale processes and interactions among them. One of particularly promising approaches is sparse space-time SP [55]. However, even with growing availability of computation resources, these methods are not currently viable for application to the large ensemble-size weather prediction or climate simulations. Thus, computationally inexpensive GCM parameterizations that capture the variability and coherent structure of the deep convection have remained a central unsolved problem in the atmospheric community.

The most common conventional cumulus parameterizations are based on the quasi-equilibrium (QE) assumption [1], the moist convective adjustment idea of [39], or the large scale moisture convergence closure of Kuo [29] type. As such, the mean response of unresolved modes on large/resolved scale variables is formulated according to various prescribed deterministic closures [16, 2,57]. These purely deterministic parameterizations were found to be inadequate for the representation of the highly intermittent and organized tropical convection [45] and many of the improvements in GCMs of the last decade came from the relaxation of the QE assumption, through the addition of a stochastic perturbation [3,31,27,35,38]. Stochastic processes have been used to parameterize convective momentum transport [38], to improve conceptual understanding of the transition to deep convection through critical values of column water vapor [52], as well as for the analysis of cloud cover data in the tropics and the extratropics [14].

A novel approach to the problem of missing tropical variability in GCMs has been the development of the multicloud parameterizations [22–26,19,5]. The multicloud parameterizations capture the interaction of three cloud types (congestus, deep and stratiform) which characterize tropical convection. The multicloud framework also includes both low-level moisture preconditioning through the second baroclinic convergence due to congestus heating and cooling and the direct effect of stratiform clouds including downdrafts which cool and dry the boundary layer. The deterministic closure takes into account the energy available for congestus and deep convection and uses a non-linear moisture switch that allows natural transitions between congestus and deep convection. The stochastic multicloud model [19,5] (hereafter KBM10 and FMK12) aims to capture these phenomena with a Markov chain lattice model where each lattice site is either occupied by a cloud of a certain type or it is a clear sky site. The convective elements interact with the large scale environment and with each other through convective available potential energy (CAPE) and middle troposphere dryness. This type of lattice model is an extension of

an Ising-type spin-flip model used for phase transitions in material science [17] and has been successfully used to improve simpler (one cloud) convective parameterizations [27,35]. When local interactions between the lattice sites are ignored, the dynamical evolution of the cloud area fractions in the stochastic multicloud model takes the form of a coarse grained stochastic process that is intermediate between the microscopic dynamics and the mean field equations [17,27,35]. The deterministic mean field limit equations (DMFLE) can be viewed as a separate deterministic parameterization within the multicloud framework (see Fig. 1) and under certain simplifying assumptions can be liked to the deterministic multicloud parameterization. The design principles of the multicloud parameterization framework are extensively explored in the deterministic version of the model developed by Khouider and Majda [22–26] (hereafter KM06a, KM06b,KM07, KM08a, KM08b, respectively).

Here, a version of the stochastic multicloud parameterization (FMK12) with a new stratiform heating closure and a congestus detrainment mechanism is studied. As in KBM10 and FMK12, the parameterization is coupled to a simplified model of the primitive equations; the vertical resolution is reduced to the first two baroclinic modes. The modifications further improve the representation of intermittent coherent structures such as synoptic and mesoscale convective systems. Single column simulations are used here to elucidate the effects of these modifications. The deterministic mean field limit equations, on the other hand, allow us to illustrate the role of stochastic processes through side-by-side comparison of stochastic and DMFLE simulations. Additional emphasis is placed on elucidating connections between deterministic, stochastic and DMFLE parameterizations of the multicloud framework. Lastly, statistical analysis of precipitation reveals qualitative agreement with observations and is used to highlight the effects of the modifications introduced here.

The rest of the paper is organized as follows. A self contained review of the deterministic multicloud parameterization is presented in Section 2. The dynamical core is thoroughly discussed in this section, as it is used in all the multicloud parameterizations presented here. In Section 3, we review the stochastic multicloud model and introduce the new stratiform heating closure and the congestus detrainment mechanism. This section also includes the derivation of the deterministic mean field limit equations and makes links with the deterministic multicloud model. In Section 4, single column simulation results are used to illustrate the effects of the two modifications listed above. In this section, we also employ the DMFLE to elucidate the role of stochastic noise in the parameterization. In Section 5, the modified parameterization is used to study flows above the equator on a moderate size GCM grid (40 km) in both aquaplanet and SST gradient regimes. A statistical analysis of the these results, with emphasis on auto-correlation function and event size distribution of precipitation, is presented in Section 5.3. In addition to qualitative agreement with observations, this study highlights in particular the improvement of the auto-correlation functions of water vapor and precipitation when the

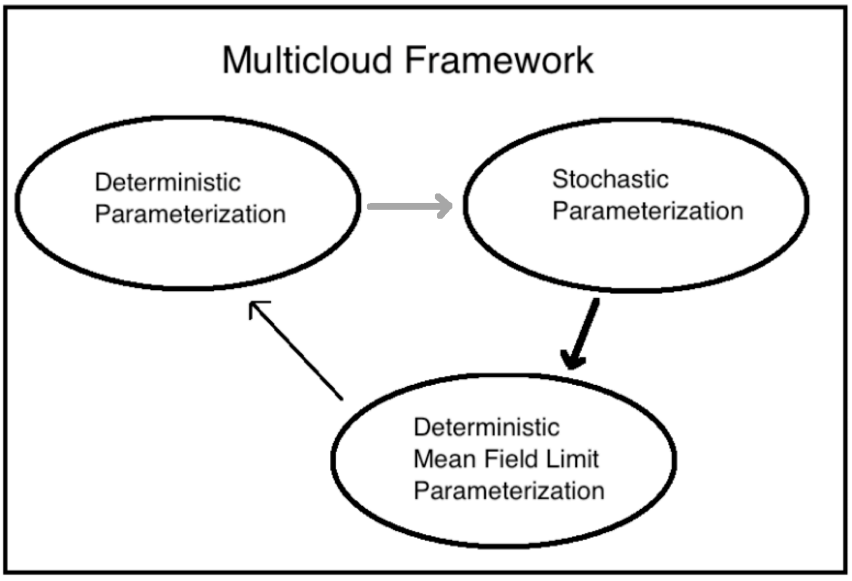

Fig. 1 Conceptual diagram of multicloud framework encapsulating the three convective parameterizations discussed in this paper. The stochastic multicloud model is built on the fundamental ideas of the deterministic multicloud model. The deterministic mean field limit (DMFL) equations are derived from the stochastic multicloud parameterization. DMFL can be used as a standalone parameterization that, in certain regimes, is capable of capturing some of the features of the stochastic parameterization. Furthermore, DMFL can be used to elucidate the role of the stochastic noise in the stochastic multicloud parameterization and under certain simplifying assumptions provides a connection to the deterministic multicloud model.

stratiform lag and congestus mechanisms are included. Some discussion and concluding remarks are given in Section 6.

2 Summary of the deterministic multicloud parameterization.

We start with a a brief review of the dynamical core equations used for both the deterministic and the stochastic multicloud parameterizations. A more thorough and detailed discussion of the model equations is found in (KM06). Nevertheless, a comprehensive list of the model constants and parameters is given in Table 1 for the sake of completeness.

2.1 Dynamical core

Both deterministic and stochastic multicloud parameterizations assume three heating profiles associated with the main cloud types that characterize organized tropical convective systems [15]: cumulus congestus clouds that heat the

lower troposphere and cool the upper troposphere, through radiation and detrainment, deep convective towers that heat the whole tropospheric depth, and the associated lagging-stratiform anvils heat the upper troposphere and cool the lower troposphere, due to evaporation of stratiform rain. Accordingly, the dynamical core of both the deterministic and the stochastic multicloud convective parameterizations used in this paper consists of two coupled and forced shallow water systems. Without the meridional dependency, the equations are given by

$$\partial_t u_j - \partial_x \theta_j = C_d u_0 u_j - \frac{1}{\tau_R} u_j, \quad j = 1, 2 \tag{1}$$

$$\partial_t \theta_1 - \partial_x u_1 = H_d + \xi_s H_s + \xi_c H_c - S_1, \tag{2}$$

$$\partial_t \theta_2 - \frac{1}{4} \partial_x u_2 = H_c - H_s - S_2. \tag{3}$$

Here H_d, H_s and H_c are the heating rates for deep, stratiform and cumulus congestus clouds obtained by either the deterministic or the stochastic parameterization. These heating rates are combined to form the bulk precipitation $P = H_d + \xi_s H_s + \xi_c H_c$. The coefficients ξ_c and ξ_s denote contribution of congestus and stratiform rain to the bulk precipitation, their role will be discussed in Sec. 3.3. The last terms of the first and second baroclinic heating mode equations, $S_j = \theta_j \tau_D^{-1} + Q_{R,j}^0, j = 1, 2$, represent radiative cooling rates. The parameters C_d and u_0 are respectively the momentum drag coefficient and the strength of turbulent fluctuations in the boundary layer.

The multicloud models additionally carry an equation for the vertically integrated tropospheric moisture content, q, and an equation for the boundary layer equivalent potential temperature, θ_{eb}. The free troposphere moisture, q, equation takes the form

$$\frac{\partial q}{\partial t} + \partial_x [(u_1 + \tilde{\alpha} u_2) q + (u_1 + \tilde{\lambda} u_2) \tilde{Q}] = -\frac{2\sqrt{2}}{\pi} P + (D + E_c)/H_T. \tag{4}$$

The coefficients $\tilde{\alpha}, \tilde{\lambda}$ and $\tilde{Q}$ of the moisture convergence term are stated in Table 1. Here the downdraft, D, is given by

$$D = m_0 [1 + \mu (H_s - H_c)/Q_{R,1}^0]^+ (\theta_{eb} - \theta_{em}). \tag{5}$$

The downdraft mass flux reference scale, m_0, is computed from radiative convective equilibrium (RCE) while, μ, the relative contribution of stratiform and congestus heating rates to downdrafts, is prescribed. The middle tropospheric equivalent potential temperature, θ_{em}, is given by

$$\theta_{em} = q + \frac{2\sqrt{2}}{\pi} (\theta_1 + \alpha_2 \theta_2). \tag{6}$$

Due to the low Bowen ratio over the ocean, the boundary layer potential temperature and moisture are combined into a single equation for the boundary layer equivalent potential temperature [23]

$$\partial_t \theta_{eb} = \frac{1}{h_b} (E - E_c - D), \tag{7}$$

where the sea surface evaporation E takes the form

$$\frac{E}{h_b} = \tau_e^{-1}(\theta_{eb}^* - \theta_{eb}). \tag{8}$$

For single column and homogeneous SST numerical experiments, the sea surface saturation equivalent potential temperature, θ_{eb}^*, is set to a constant , so that $\bar{\theta}_{eb}^* - \bar{\theta}_{eb} = 10K$. Here and throughout the paper, $\bar{X}$ denotes the RCE value of the variable X. In the (x,t) simulations where SST is not homogenous, the sea surface saturation equivalent potential temperature takes the form

$$\theta_{eb}^*(x) = 5\cos\left(\frac{4\pi x}{40000}\right) + 10K, \tag{9}$$

within an interval of 20,000 km of the 40,000 km domain and $\theta_{eb}^* = 5$ K everywhere else as in Khouider and Majda (2007) and KM08a. This setup mimics the Indian Ocean–Western Pacific warm pool.

The term E_c, which appears in Eq. 4 and 7 is a new feature introduced in this paper. It accounts for the detrainment of congestus clouds, which serves to moisten the free troposphere and dry the boundary layer. This is discussed in more detail in Sec. 3.3. However, it is important to note at this stage that the addition of the congestus detrainment moistening effects does not interfere with the conservation of vertically averaged moist static energy.

2.2 Deterministic multicloud parameterization

One of the ideas behind the deterministic multicloud parameterization (KM06) lies in the introduction of the nonlinear switch Λ, which serves as a measure for the moistness and dryness of the middle troposphere. When the discrepancy between the boundary layer and the middle tropospheric equivalent potential temperature is larger than a threshold value θ^+ the atmosphere is defined as dry and the switch value is set to 1. Moist parcels rising from the boundary layer will have their moisture quickly diluted by entrainment of dry air, hence losing buoyancy and stop convecting. In such situations, cumulus congestus clouds are favored. When this discrepancy is below some lower value, θ^-, the atmosphere is defined as moist and deep convection is favored. An extensive discussion of of the switch and the choice of threshold values can be found in KM06. The function Λ is then interpolated (linearly) between these two values. Formally, the equation takes the form (KM06)

$$\Lambda = \begin{cases} 1 & \text{if } \theta_{eb} - \theta_{em} > \theta^+ \\ A(\theta_{eb} - \theta_{em}) + B & \text{if } \theta^- \le \theta_{eb} - \theta_{em} \le \theta^+ \\ 0 & \text{if } \theta_{eb} - \theta_{em} \le \theta^-. \end{cases} \tag{10}$$

The "energy" available for deep convective heating is given by (KM06)

$$Q_d = \bar{Q} + \tau_{conv}^{-1}[a_1\theta_{eb} + a_2 q - a_0(\theta_1 + \gamma_2\theta_2)]^+. \tag{11}$$

It has three main components. Deep convection is favored by the increase in θ_{eb} and q and decrease in $(\theta_1 + \gamma_2\theta_2)$. Thus, convection is favored by the increase in boundary layer moisture as in a CAPE parameterization, and tropospheric moisture content as in Betts-Miller [2] type parameterization. Furthermore, colder middle troposphere facilitates deep convection by allowing saturation at weaker mixing ratios [23], through the dry convective buoyancy parameter a_0. The same expression is used in the parameterization of deep convective heating and CAPE for the stochastic multicloud model. Meanwhile, the parameterization for bulk energy available for congestus clouds can be formally obtained by integrating over the lower troposphere, the convective buoyancy anomaly of a dilute parcel raised from the boundary layer constantly mixing with the environment (KM08a). The equation takes the form,

$$Q_c = \bar{Q} + \tau_{conv}^{-1}[\theta_{eb} - a_0'(\theta_1 + \gamma_2'\theta_2)]^+. \tag{12}$$

Note that Q_c does not depend on vertically integrated atmospheric moisture. It is mainly driven by the boundary layer and has a high sensitivity to the second baroclinic potential temperature through high value of $\gamma_2' = 2$ [26]. This reflects the sensitivity of congestus clouds to the variation in the lower tropospheric temperature, the region where congestus clouds are active. This quantity is effectively equivalent to the definition of low level CAPE in the stochastic multicloud model.

The dynamics of congestus and stratiform heating are expressed through two lag type differential equations, while deep convective heating is obtained through a diagnostic equation.

$$\frac{\partial H_c}{\partial t} = \frac{1}{\tau_c}(\alpha_c \Lambda Q_c^+ - H_c) \tag{13}$$

$$H_d = (1 - \Lambda)Q_d^+ \tag{14}$$

$$\frac{\partial H_s}{\partial t} = \frac{1}{\tau_s}(\alpha_s H_d - H_s) \tag{15}$$

In this context, the nonlinear switch allows congestus heating dynamics to adjust dynamically to a fraction of low level CAPE. At the same time, the nonlinear switch allocates a fraction of CAPE to deep convection through an algebraic closure. Lastly, stratiform heating adjusts towards a fraction of the deep convective heating. The incorporation of a stochasticized version of the lag type stratiform heating closure into the stochastic multicloud model, as discussed in Sec. 3.2, leads to a net improvement of the stochastic multicloud model. It is important to note that the interactions between dryness, CAPE and low level CAPE play an important role in the stochastic multicloud model.

The dynamical features and capabilities of the deterministic multicloud parameterization, in terms of the impact on the large scale tropical circulation and convectively coupled waves are demonstrated in Khouider and Majda (KM06a, KM06b,KM07, KM08a, KM08b), using both linear analysis and non-linear simulations. In the appropriate parameter regime, the deterministic

multicloud model is very successful in capturing most of the Wheeler-Kiladis-Takayabu spectrum of convectively coupled waves [53, 54] in terms of linear wave theory (KM06a;KM08b; [10]) and nonlinear organization of large-scale envelopes mimicking across-scale interactions of the Madden-Julian oscillation (MJO) and convectively coupled waves (KM07; KM08a; [37]), in the idealized context of a simple two-baroclinic modes model employed here. Furthermore, the parameterization has been used in the next generation of the National Center for Atmospheric Research GCM (HOMME) and is revealed to be successful in simulating the MJO and convectively coupled equatorial waves, at a coarse resolution of 170 km, in the idealized case of a uniform SST (aquaplanet) setting [28].

However, the sensitivity of the deterministic multicloud model to the key parameters means that in some physically motivated parameter regimes, such as the physical regime used for the stochastic parameterization in this study, the model can perform poorly. In FMK12, such poor choice of parameters was taken to provide a reference point that roughly corresponds to the behavior of a paradigm GCM parameterization with clear deficiencies. In particular, it was shown that simulations in the suboptimal regime can give rise to extremely regular convectively coupled waves that moved with a fast speed and lacked vertical tilting. This was mainly due to a lowered convective buoyancy frequency, which allowed a large amount of deep convection and nullified the effects of congestus and stratiform heating, which are responsible for the vertical tilt and are believed to be crucial for a correct propagation speed. Furthermore, Walker cell type simulations showed unphysical mean circulation structure, which weakly interacted with the waves described above (FMK12).

Another example of oversensitivity to parameters can be found in KM08a. A well-tuned model, that produces MJO like structures and coherent waves with the correct propagation speed, responds to the increase in mean dryness by producing a wave number one circulation. Unlike typical Walker cell, this circulation has sharp congestus peaks at the boundary between the active and the inactive convective regions, which are not observed in nature. The authors, in FMK12, have shown that the stochastic parameterization can overcome some of these sensitivity issues. This idea will be further reinforced in Section 5.

3 The stochastic multicloud model

3.1 Stochastic parameterization

Just like the deterministic multicloud model, the stochastic multicloud parameterization is designed to capture the dynamical interactions between the three cloud types that characterize organized tropical convection and the environment. In the stochastic multicloud model these interactions are represented through a coarse grained lattice model (KBM10). To mimic the behavior within a typical GCM grid box, a rectangular n x n lattice is considered.

Table 1 Constants and parameters common to all multicloud parameterizations discussed in this paper. The deviations from these values in congestus moistening mechanism simulations are discussed in Section 3.3

Parameter	Value	Description
$h_b/H_m/H_T$	500 m / 5 km/ 16 km	ABL depth/ average depth of the mid-troposphere/ Free troposphere depth
Q_{R1}	1 K/day	First baroclinic radiative cooling rate
Q_{R2}	Determined at RCE	Second baroclinic radiative cooling rate
ξ_s/ξ_c	0.4/0	Stratiform/Congestus contribution to first baroclinic mode
$\tilde{Q}$	0.9	Background moisture stratification
$\tilde{\lambda}/\tilde{\alpha}$	0.8/0.1	Coefficient of u_2 in linear / nonlinear moisture convergence
m_0	Determined at RCE	Large-scale background downdraft velocity scale
μ	0.25	Contribution of convective downdrafts to D
α_s/α_c	0.25/ 0.1	Stratiform/Congestus adjustment coefficient
τ_R/τ_D	75 days / 50 days	Rayleigh drag / Newtonian cooling time scale
τ_s/τ_c	3 hours / 2 hour	Stratiform /Congestus adjustment time scale
τ_{conv}	2 hours	Convective time scale
τ_e	Determined by RCE	Surface evaporation time scale
$\bar{Q}$	Determined at RCE	Bulk convective heating at RCE
$\bar{\theta}_{eb} - \bar{\theta}_{em}$	11 K	Mean (RCE) Dryness of the atmosphere
θ^-/θ^+	10 K /20 K	Deterministic moisture switch threshold values
A/B	1/0	Deterministic moisture switch parameters
a_1/a_2	0.45 / 0.55	Relative contribution of θ_{eb} / q to deep convection
a_0/a_0'	2 / 1.5	Dry convective buoyancy frequency in deep/congestus heating equations.
γ_2/γ_2'	0.1 / 2	Relative contribution of θ_2 to deep /congestus heating
α_2	0.1	Relative contribution of θ_2 to θ_{em}
C_d	0.001	Surface drag coefficient
u_0	2 m/s	Strength of turbulent fluctuations
$CAPE_0$	400 J/Kg	Reference values of CAPE
T_0	12 K	Reference values of dryness
$\bar{\alpha}$	$\approx$ 15 K	Unit scale of temperature

Table 2 Transition rates and time scales in the stochastic and deterministic mean field limit parameterizations (deviations from these values in congestus moistening mechanism simulations are discussed in section 3.3) . Here $\Gamma(x) = 1 - \exp(-x)$ for $x > 0$ and zero otherwise, $C_l = CAPE_l/CAPE_0$,$C = CAPE/CAPE_0$ and $D = (\theta_{em} - \theta_{eb})/T_0$.

Transition Rate	Time scale (h)	
Formation of congestus	$R_{01} = \frac{1}{\tau_{01}}\Gamma(C_l)\Gamma(D)$	τ_{01}=1
Decay of congestus	$R_{10} = \frac{1}{\tau_{10}}\Gamma(D)$	τ_{10}=1
Conversion of congestus to deep	$R_{12} = \frac{1}{\tau_{12}}\Gamma(C)(1-\Gamma(D))$	τ_{12}=1
Formation of deep	$R_{02} = \frac{1}{\tau_{02}}\Gamma(C)(1-\Gamma(D))$	τ_{02}=3
Conversion of deep to stratiform	$R_{23} = \frac{1}{\tau_{23}}$	τ_{23}=3
Decay of deep	$R_{20} = \frac{1}{\tau_{20}}(1-\Gamma(C))$	τ_{20}=3
Decay of stratiform	$R_{30} = \frac{1}{\tau_{30}}$	τ_{30}=5

Each element of the lattice is occupied by a congestus, deep or a stratiform cloud or is a clear sky site. It is represented by an order parameter that takes accordingly the values 0,1,2 or 3. A continuous time stochastic process is then defined by allowing the transitions, for individual cloud sites, from one state to another according to intuitive probability transition rates, which depend on the large scale-resolved variables. These large scale variables are the convective available potential energy integrated over the whole troposphere (CAPE),

$$CAPE = \overline{CAPE} + R(\theta_{eb} - \gamma(\theta_1 + \gamma_2\theta_2)), \tag{16}$$

the convectively available energy integrated over the lower troposphere CAPE_l

$$CAPE_l = \overline{CAPE} + R(\theta_{eb} - \gamma(\theta_1 + \gamma_2'\theta_2)), \tag{17}$$

and the dryness of the mid troposphere, which is a function of the difference between the atmospheric boundary layer (ABL) temperature θ_{eb} and the middle tropospheric potential temperature θ_{em}. In Eqns 16 and 17, $\gamma = 1.7$ is the dry lapse rate, while the role of γ_2 and γ_2' is discussed in Section 2.2. The inclusion of the dryness of the middle troposphere accounts for mixing of the convective parcels with dry environmental air (KM06a, KM06b,KM07, KM08a, KM08b,KBM10) and is conceptually similar to the switch Λ in the deterministic multicloud model, as discussed in the previous section.

The probability rates are constrained by a set of intuitive rules which are based on observations of cloud dynamics in the tropics (e.g. [15,40], KM06a, and references therein). Following KBM10, a clear site turns into a congestus site with high probability if low level CAPE is positive and the middle troposphere is dry. A congestus or clear sky site turns into a deep convective site with high probability if CAPE is positive and the middle troposphere is moist. A deep convective site turns into a stratiform site with high probability. Finally, all three cloud types decay naturally to clear sky at some fixed rate. All other transitions are assumed to have negligible probability. These rules are formalized in Table 2 in terms of the transition rates R_{ik} and the associated time scales τ_{ik}. The effects of CAPE and dryness enter the model with scaling parameters $CAPE_0$ and T_0 whose values are specified in sections 3.2 and 3.3, namely through

$$C_l = CAPE_l/CAPE_0 \tag{18}$$

$$C = CAPE/CAPE_0 \tag{19}$$

$$D = (\theta_{em} - \theta_{eb})/T_0 \tag{20}$$

and the exponential function

$$\Gamma(x) = \begin{cases} 1 - \exp(-x) & \text{if } x > 0 \\ 0 & \text{otherwise.} \end{cases} \tag{21}$$

Notice that the assumption that the transition rates depend on the large scale variables accounts for the feedback of the large scales on the stochastic model, while ignoring the interactions between the lattice sites all together implies that the stochastic processes associated with the different sites are identical

(independent and identically distributed). The latter simplification makes it easy to derive the stochastic dynamics for the GCM grid box cloud coverage alone, which can be evolved without the detailed knowledge of the micro-state configuration, by using a coarse-graining technique [17,18] that yields here a system of three dimensional birth-death stochastic process for the congestus, deep and stratiform cloud fractions σ_c, σ_d and σ_s respectively.

As in KBM10 and FMK12, the heating associated with congestus and deep clouds is assumed to be proportional to the cloud fraction according to the following closure equations.

$$H_c = \sigma_c \frac{\alpha_c \bar{\alpha}}{H_m} \sqrt{CAPE_l^+}, \tag{22}$$

$$H_d = [\sigma_d \bar{Q} + \frac{1}{\tau_c(\sigma_d)}(a_1\theta_{eb} + a_2 q - a_0(\theta_1 + \gamma_2\theta_2))]^+, \tag{23}$$

$$\tau_c(\sigma_d) = \frac{\bar{\sigma_d}}{\sigma_d}\tau_c^0, \tag{24}$$

where $\bar{\sigma}_c, \bar{\sigma}_d$ and $\bar{\sigma}_s$ denote the radiative convective equilibrium (RCE) values of the congestus, deep and stratiform cloud area fractions. We note that, just like in the deterministic multicloud model, the congestus heating is tied to the low level CAPE, while, deep convective heating is tied to overall CAPE. However, unlike the nonlinear switch of the deterministic multicloud model, the cloud fractions (of congestus and deep convective clouds) are dependent on both CAPE and dryness. This extra dependency, among other factors, contributes to the strong nonlinearity exhibited by the stochastic multicloud model and subsequently the deterministic mean field equations.

While, as discussed below, one crucial modification introduced in this paper is the new stratiform heating closure, it is important to recall that in FMK12 the following closure was introduced and used. It is more consistent with the CAPE–Betts–Miller parameterization used for deep convection.

$$H_s = \alpha_s[\sigma_s \bar{Q} + \frac{1}{\tau_c(\sigma_s)}(a_1\theta_{eb} + a_2 q - a_0(\theta_1 + \gamma_2\theta_2))]^+, \tau_c(\sigma_s) = \frac{\bar{\sigma_s}}{\sigma_s}\tau_c^0. \tag{25}$$

Here $\bar{\sigma}_s$ is the fraction of stratiform rain at RCE. The creation of stratiform rain is directly tied to the deep convective cloud population and by design the FMK12 stratiform heating closure was functionally similar to the deep convective heating closure (23). The new stratiform heating closure is discussed next.

3.2 New stochastic lag heating closure

One important modification to the stochastic multicloud model done in this paper is the introduction of a new stratiform heating closure. Instead of the algebraic stratiform heating closure (25), the current model uses a lag-type ordinary differential equation (ODE) for the stratiform heating dynamics. This

type of closure is similar to the one used in the deterministic multicloud model, (15), but it takes into account the stochastic effects of the stratiform cloud fraction. This closure is used to enhance synchronization between stratiform heating and cloud fractions and appears to be necessary for the successful implementation of the congestus detrainment mechanism of the next section.

Similarly to the stratiform heating closure of the deterministic multicloud model, the new stratiform heating closure is given by

$$\partial_t H_s = \frac{1}{\tau_s}(\alpha_s \sigma_s H_d/\bar{\sigma}_d - H_s). \tag{26}$$

Where τ_s and α_s are the stratiform adjustment time scale and the stratiform fraction of deep convection, respectively. Through the deep convective heating term, H_d, the deep convective cloud fraction enters the stratiform heating equation, which provides additional coherence to the heating fields. The new closure results in RCE solutions identical to the ones obtained with the diagnostic stratiform heating closure in (25).

As it will be illustrated in the next section, this crucial change, greatly improves the synchronization of stratiform heating and cloud fractions in the single column simulation. In the spatially extended simulations, this change results in greater coherence of stratiform and congestus heating fields of convectively coupled waves. It is used in all simulations in this paper (except for the results taken from FMK12) including the simulations with the congestus detrainment mechanism, which is discussed next.

3.3 Moistening by Congestus Detrainment

A recent CRM study, by Waite and Khouider (2010), suggests that about 2 g/kg of moistening by congestus clouds during the preconditioning and transition phase to deep convection is due to direct detrainment of congestus clouds in the lower to middle troposphere in addition to large scale low-level convergence associated with low-level congestus heating. While the congestus detrainment is included in the multicloud models as part of the upper level cooling, its direct moistening effect was not taken into account. Here we attempt to add such a process to the multicloud model framework.

As a first and simple model, the moistening by congestus detrainment is assumed to be proportional to the congestus cooling above the freezing level. It is important to note that we have chosen to disregard congestus precipitation, by setting $\xi_c = 0$ for all simulations in this paper. Thus, congestus cooling above the freezing level is equal to the congestus heating bellow. This allows us to ignore the effects of the congestus downdraft mass flux due to the congestus precipitation. Thus, the congestus detrainment moistening in our model refers to the effect of vigorous shallow updrafts that entrain large amounts of boundary layer air and transport it into the free troposphere. It is parameterized through the term E_c in Eq. (2.4) and (2.7) and which takes

the form:

$$E_c = \frac{\sqrt{2}}{\pi} \frac{H_c}{Q^0_{R,1}} (\theta_{eb} - \theta_{el}), \tag{27}$$

i.e., the air mass flux is a product of the scaled congestus heating rate and the difference between equivalent potential temperatures in the boundary layer and the lower troposphere, $\theta_{eb} - \theta_{el}$. At RCE, $\bar{\theta}_{eb} - \bar{\theta}_{el}$ is set to 2 K, while for the deviations from the RCE we set

$$\theta_{el} = 2q + \frac{2\sqrt{2}}{\pi}(\theta_1 + 2\theta_2). \tag{28}$$

Consistent with the two baroclinic model approximation, Eq. (3.29) is obtained by averaging the total heating and moisture fields over the lower troposphere, where congestus clouds develop, expanding roughly between the top of the boundary layer and the middle of the free troposphere, $H_T/2$, (representing roughly the freezing level). This is similar to the computation of θ_{em} in KM06 but we additionally exploit the fact that moisture fluctuations are bottom heavy and the value of the coefficient of the second baroclinic mode is higher. It is in fact equal to the weight of the second baroclinic mode in the low level CAPE (KM08a).

The entrainment term E_c/H_T in the moisture equation (4) is understood as the entrainment of cloudy air into environmental air and thus serves to moisten the environment, while E_c/h in the boundary layer equation (7) models the entrainment of dry free-tropospheric air into the boundary layer by the turbulent eddies due to congestus updrafts. These two entrainment terms are assumed to balance each other (when vertically averaged, i.e, when the mass of the two air columns is taken into account).

For these simulations, we alter the standard values of the parameters (listed in Tables 1 and 2) in the following way. First, the dryness of the troposphere, $\bar{\theta}_{eb} - \bar{\theta}_{em}$, is set to the higher value of 15K to increase the formation of congestus clouds. To strengthen the nonlinearity we set CAPE threshold to $CAPE_0 = 400$ J/ kg and double the value of relative contribution of stratiform evaporative cooling to downdrafts by setting $\mu = .5$. We also use a faster congestus to deep cloud transition time scale, $\tau_{12} = .25$ hour, and a slightly lower value for the decay time scale of deep convective clouds, $\tau_{20} = 2$ hours. Lastly, we include the effects of moisture by incorporating it into the CAPE equation by setting

$$CAPE = \overline{CAPE} + R(\theta_{eb} + a_2' q - \gamma(\theta_1 + \gamma_2 \theta_2)), \tag{29}$$

where $a_2' = 0.7$ serves similar purpose to coefficient a_2 in equation (23).

As it will be shown in Sections 4 and 5, the congestus detrainment mechanism is of paramount importance to the stochastic multicloud model. In the stochastic multicloud model, this process leads to parameterized dynamics driven by the intrinsic deterministic chaos. This can be deduced from the deterministic mean field limit equations of the stochastic multicloud model, which is presented next.

3.4 The deterministic mean field limit equations and connections to the deterministic multicloud model

As derived in KBM10, the deterministic mean field limit equations (DMFLE) take the form:

$$\dot{\sigma_c} = \sigma_{cs} R_{01} - \sigma_c (R_{10} + R_{12}) \tag{30}$$

$$\dot{\sigma_d} = \sigma_{cs} R_{02} + \sigma_c R_{12} - \sigma_d (R_{20} + R_{23}) \tag{31}$$

$$\dot{\sigma_s} = \sigma_d R_{23} - \sigma_s R_{30} \tag{32}$$

While, the equations (30)-(32) appear deceptively simple, it is important to note that the transition rates $R_{i,k}$ are exponential functions of dryness, $CAPE$ and $CAPE_l$, as stated in Table 2. Thus, when coupled to the large scale dynamics, the deterministic mean field limit equations are strongly nonlinear and thus can display chaotic behavior. This is particularly the case when congestus detrainment moistening is included, as demonstrated below. The DMFLE model also allows us to elucidate the role of stochastic fluctuations in the model and weigh them against the deterministic chaos.

Further, as discussed previously in Section 2.2, in the deep convective heating equations of the stochastic parameterization, cloud fraction is used in a manner analogous to the nonlinear switch of the deterministic multicloud model. However, the nonlinear switch is a function of dryness only, whereas the cloud fractions are dependent (through the transition rates listed in Table 2) on both CAPE and dryness. This extra dependency, among other factors, contributes to the strong nonlinearity exhibited by the stochastic multicloud model. It is possible to make connections between the DMFLE and the heating closures of the deterministic multicloud model by considering a regime where the dependency of the cloud fractions on CAPE (and low level CAPE) is suppressed.

In order to facilitate the comparison with the deterministic multicloud model, we consider a scenario where the cloud fraction transition rates are determined by fluctuations in dryness alone. In fact, as shown in Appendix 1, we can rewrite the equation for the evolution of congestus heating in a simpler and more familiar form,

$$\dot{H}_c \approx \frac{1}{\tau_c^{MFL}} (\alpha_c^{MFL} \Gamma(D) \sqrt{CAPE_l^+} - H_c) \tag{33}$$

where

$$\tau_c^{MFL} = \frac{\tau_{12}}{\Gamma(\bar{C})} \alpha_c^{MFL} = \alpha_c \frac{\tau_{12} \bar{\alpha}}{\tau_{01} H_m}. \tag{34}$$

Here, $\bar{C}$ denotes RCE value of C in equation (16). Equation (33) is analogous to the equation for congestus heating in the deterministic multicloud model, namely Eq. 13. Here, $\Gamma(D)$ behaves in a way that mimics the nonlinear switch in the deterministic model. Like the deterministic switch Λ, $\Gamma(D)$ tends to zero when the troposphere is moist (value of D is low). When the middle troposphere is dry both $\Gamma(D)$ and Λ tend to 1, favoring congestus heating.

It is also possible to make connection between the dynamics of deep convective heating of the DMFL equations and the deterministic multicloud model. As shown in Appendix 1, under assumption that the adjustment of deep convective cloud fraction is instantaneous, the deep convective heating is given approximately by

$$H_d \approx \left[\frac{\tau_{23}\tau_{20}\Gamma(\bar{C})}{\tau_{02}(\tau_{20}+\tau_{23}(1-\Gamma(\bar{C}))}\right]\left(1-\Gamma(D)\right)\left[\bar{Q}+\frac{1}{\tau^0_{conv}\bar{\sigma_d}}(a_1\theta_{eb}+a_2 q-a_0(\theta_1+\gamma_2\theta_2))\right]^+. \tag{35}$$

Aside from the constant coefficient in front, the dynamics of deep convective heating under these simplifications is similar to that of the deep convective heating of the deterministic multicloud model, (14). The behavior of the quantity $1-\Gamma(D)$ is similar to that of $1-\Lambda$ in the deterministic multicloud model. Thus, under these simplifying assumptions, congestus, deep and (by design) stratiform heating fields of the DMFLE parameterization mimic the behavior of the deterministic multicloud model. However, the extra dependency of the stochastic and the DMFLE models on CAPE results in highly nonlinear dynamics that are more realistic.

4 Single column simulations

In this section, the effects of the new mechanisms, stratiform lag closure and congestus detrainment, are studied in the context of single column simulations and compared to the FMK12 results. Both the stochastic multicloud model and the deterministic mean field limit equations are considered.

The single column equations are obtained by disregarding spatial dependence components and the zonal wind. As in KBM10, we employ a third order Adams-Bashforth method to integrate the dynamical core ODEs. The coarse grained birth-death process is evolved in time by means of Gillespie's exact algorithm (Gillespie 1975, 1977). To produce time series for the DMFLE, we employ an off-the-shelf stiff ODE solver, namely, the routine ode23s of Matlab. All simulations in this section are run for 100 days, while a 5 to 10 days interval of the solution is shown.

4.1 Stochastic simulations

To facilitate the comparison, we first review the basic results of FMK12. Left panels of Figure 2 show the stochastic simulation of FMK12. The most notable feature is the time synchronization of the oscillations of the stochastic and deterministic variables which leads to time series with frequent precipitation peaks of 10 K/Day and more intermittent large precipitation events on the order of 20 K/Day. Each convective even is initialized by a build up of low level CAPE. The resulting congestus clouds moisten the atmosphere. This moist atmosphere, combined with the build up of CAPE, produces deep

convective events which are in turn followed by stratiform clouds. The relationship between small and large precipitation events is reminiscent of a progressive deepening of convection on multiple scales (Mapes et al. 2006). By design, the congestus clouds are followed by deep convective and trailing stratiform clouds. However, while congestus and deep heating rates behave just like the cloud fractions, stratiform heating does not follow the shape of the stratiform fraction profile. While the stratiform cloud fraction lags behind deep convection, the stratiform heating is initiated before the deep convective heating.

The right panels of Figure 2 present the single column simulations in the same parameter regime as in FMK12 but with the lag type ODE stratiform closure. We note that the stratiform heating now the deep convection instead of slightly preceding it. Thus, the addition of the stochastic lag type closure greatly improves the synchronization of the stratiform heating and stratiform cloud fraction with minimum effects on the desirable features described above. Both simulations are carried out with 900 ($n = 30$) cloud sites and the simulations with the new stratiform heating closure could be said to be less intermittent. To boost the intermittency of the time series, we lower the number of convective elements. This simulation is repeated in the left column of figure 3 with $n = 10$. Despite the fact that only 100 cloud sites are used (and individual cloud transitions can be observed), the synchronization between all the variables remains. This strategy will be repeated, with great success, in the (x, t) simulations.

The congestus detrainment mechanism is the second major modification of the multicloud model introduced in this paper. The deviations in parameter regime from the standard values used in Table 1 and 2 are described in section 3.3 and it should be emphasized that the new stratiform closure is also used for the simulation. The resulting time series, right column of Figure 3, is characterized by prolonged periods of congestus activity induced by fluctuations in low-level CAPE and atmospheric dryness. The effect of congestus preconditioning can be clearly seen in the increase of moisture anomalies, q, and in the reduction in the dryness, D. The congestus preconditioning phase is typically followed by a large deep convective event associated with a build up of CAPE. This deep convective event consumes CAPE and dries the atmosphere setting up the environment for the next cycle. This regime is characterized by very large fluctuations in CAPE_l, CAPE and D.

4.2 Deterministic Mean Field Limit simulations

In Section 3.4, we derived the deterministic mean field limit equations for the stochastic multicloud model. Here, we run simulations with the DMFLE to elucidate the role of the stochastic and intrinsic deterministic chaos in the stochastic multicloud model. As discussed in 3.4, the DMFLE parameterization can be reduced with a few simplifying assumptions to a form that is similar to the deterministic multicloud mode. However, the full DMFL pa-

rameterization is highly nonlinear and in certain regimes captures some of the chaotic features of the stochastic parameterization. The simulations of FMK12, new stratiform heating and congestus detrainment regimes form three distinct examples, which highlight the role of the stochastic noise in the multicloud model.

First, we show on the second panel of Figure 4 the DMFLE with the FMK12 parameter regime without the new stratiform heating closure. Unlike the stochastic simulation of FMK12 shown on the first panel, the DMFLE simulation is characterized by a regular cycle of oscillations with a period of roughly two days. Small convective peaks of roughly 10K/day are followed by larger 20K/day convective peak. It can therefore be surmised that the stochastic noise is the driving force of the robust intermittency in the FMK12 simulations.

When the new stratiform heating closure is considered, the DMFLE simulations exhibit more variability, as can be see in the fifth panel of Figure 4. The new model produces a variety of convective events ranging from 10 to 18 K/Day with no obvious correlation pattern. In terms of structure and variability, the DMFLE simulation is comparable to the stochastic simulation with 900 convective sites $n = 30$ (fourth panel of the same figure). By lowering the number of convective sites, we effectively increase the amount of the stochastic noise in the model and improve upon the intrinsic deterministic variability of the system. It is interesting to note that, with the FMK12 stratiform heating closure, setting $n = 30$ produces much more "chaotic" behavior. Thus, the number of convective sites is a good measure of the strength of the stochastic noise only for some particular parameter regime.

The two bottom panels of Figure 4 present the single column simulation for the regime with congestus detrainment moistening. It can be seen (by comparing the two bottom panels) that both stochastic and DMFLE simulations are characterized by prolonged periods of congestus activity, which serve to moisten and precondition the environment for deep convection. This complex and seemingly chaotic behavior comes from the DMFLE. It can be linked to the fact that low level CAPE, CAPE and dryness all exhibit high variability, as can be seen from the bottom right panel of the Figure 3. However, the DMFLEs are stiff in this parameter regime, which is not uncommon for deterministic mean field limits of this type of lattice stochastic processes [36]. The stochastic parameterization is cheaper to evolve and offers additional noise (which does not interfere with the deterministic features of the system).

The DMFLEs are a valuable tool, which allows us to elucidate the role of the stochastic processes in the multicloud model framework. As it is illustrated in this section, the results can often be surprising. In some regimes, the DMFLE can be viewed as a "standalone" deterministic parameterization that captures some of the features of the stochastic parameterization. Albeit, in these highly nonlinear regimes, the DMFLE parameterization might be computationally impractical.

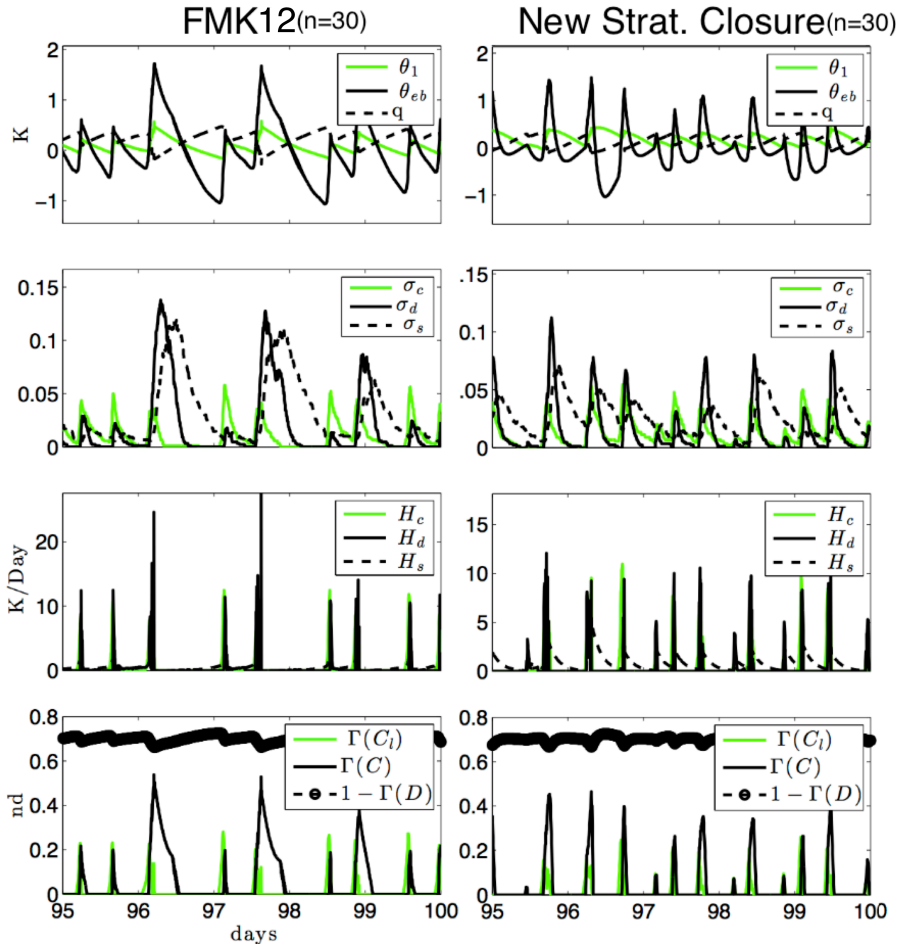

Fig. 2 Time evolution of a single column simulation for FMK12 (left) and new stratiform heating closure (right). Both simulations use 900 cloud sites ($n = 30$). The parameters are as in Tables 1 and 2 and are the same as in the standard parameter regime of FMK12. The top panels show a selection of the large-scale prognostic variables (top panels), the cloud area fractions and heating fields are plotted in the second and third panels, $\Gamma(C_l), \Gamma(C)$ and $1 - \Gamma(D)$ are shown at the bottom.

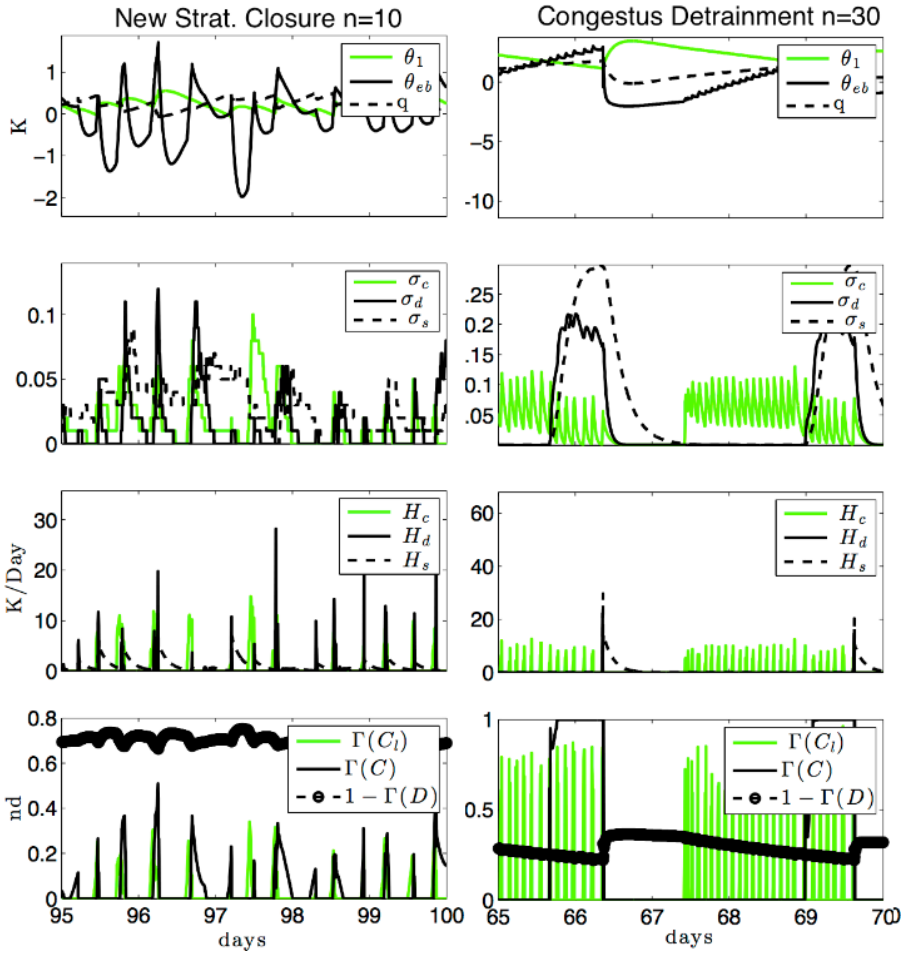

Fig. 3 Time evolution of a single column simulation for the new stratiform heating closure with a low number (n=10) of convective sites (left) and congestus detrainment regime with n=30 (right). For the new stratiform heating closure simulation, the parameters are taken as in Tables 1 and 2 and are the same as standard parameter regime of FMK12. Parameter modifications for the congestus detrainment regime are discussed in Section 3.3. The top panels show a selection of the large-scale prognostic variables (top panels), the cloud area fractions and heating fields are plotted in the second and third panels, $\Gamma(C_l), \Gamma(C)$ and $1-\Gamma(D)$ are shown at the bottom.

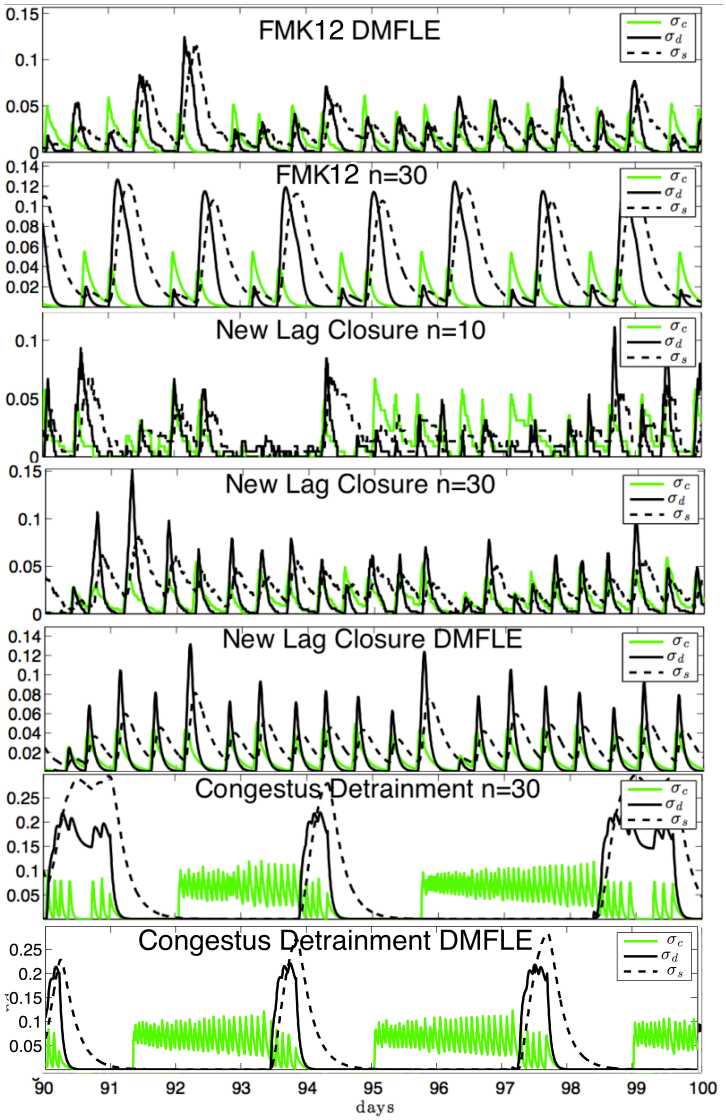

Fig. 4 Time evolution of heating profiles for various stochastic and deterministic mean field limit equation (DMFLE) simulations (top to bottom): stochastic (n=30) simulation of FMK12, DMFLE of FMK12, new lag closure with (n=10),new lag closure with (n=30), new lag closure with DMFLE, Congestus detrainment with (n=30), Congestus detrainment with DMFLE

5 Spatially extended simulations

This section presents the results of (x, t) simulations for the stochastic multicloud model with uniform and non-uniform SST backgrounds, mimicking the Indian Ocean western Pacific warm pool (Section 2.1). Simulations with the new stratiform closure and with congestus detrainment moistening mechanism are considered and compared to FMK12 and deterministic multicloud model results.

We use an operator time-splitting strategy where the conservative terms are discretized and solved by a non-oscillatory central scheme while the remaining convective forcing terms are handled by a second-order Runge-Kutta method [20,21]. As for the single column simulations, the stochastic component of the scheme is resolved using Gillespie's exact algorithm [6]. For the DMFL simulations, a second order Runge-Kutta is utilized. We consider the same parameter regimes discussed in the previous section.

5.1 Homogenous SST background

The left panels of Figure 5 show the stochastic multicloud simulation taken directly from FMK12. As pointed out in that paper, the characteristic features of the simulation are the persistent cloud decks. The congestus cloud decks appear intermittently and persistently in space and time, while generating convectively coupled gravity waves. Although the average lifespan of the convectively coupled waves is only on the order of a week, these waves travel far enough to interact with other convectively coupled waves triggered by different cloud decks. This results in a variety of convective events of different scales and magnitudes. These intermittent coherent short-lived structures, considered in detail in FMK12, are one of the great improvements over the variability of the deterministic multicloud model.

The simulations with the new stratiform closure are given on the right panels of Figure 5. Aside from the stratiform closure, all equations and parameters are inherited from FMK12, including $n = 30$. By comparing the right and the left panels of the figure, we note that waves on the right are more coherent in terms of the structure of congestus and stratiform heating fields. In addition to the synchronization of stratiform heating and stratiform cloud fractions, the coherence of the congestus heating field is greatly improved compared to FMK12. The stochastic parameterization greatly improves upon the results of the deterministic multicloud parameterization in this parameter regime, as exemplified by Figure 2 of FMK12, referred to as a paradigm example of a GCM with clear deficiencies.

The small reduction in variability, associated with the new stratiform heating closure, which was predicted by the single column studies, is remedied slightly by lowering the number of the lattice sites to $n = 10$, as done on the left panels of Figure 6. This results in an increase in the small scale variability. Overall, the addition of the lag type stratiform heating closure leads to an

improved coherence of convectively coupled waves. This comes at slight loss of the variability (when the same number, $n = 30$, of convective elements is used). However, the model still outperforms its deterministic counterpart in terms of variability of heating field and improves the representation of convectively coupled waves. The DMFLE simulation produces results similar to $n = 30$.

Lastly, the right panels of Figure 6 present the $x - t$ simulations of the congestus detrainment moistening regime for the stochastic multicloud model ($n = 30$). The model produces coherent wave structures, similar to the convective features of the stochastic multicloud model with the new stratiform heating closure. As was the case in the single column simulation, the wave structures have a strong congestus component. The convectively coupled waves move westward with a speed of approximately 17 m/s. The DMFLE simulations are not considered due to numerical stiffness. Much like the case of the paradigm example of a GCM with clear deficiencies in FMK12, the deterministic multicloud model with congestus detrainment fails to produce physical results in this parameter regime.

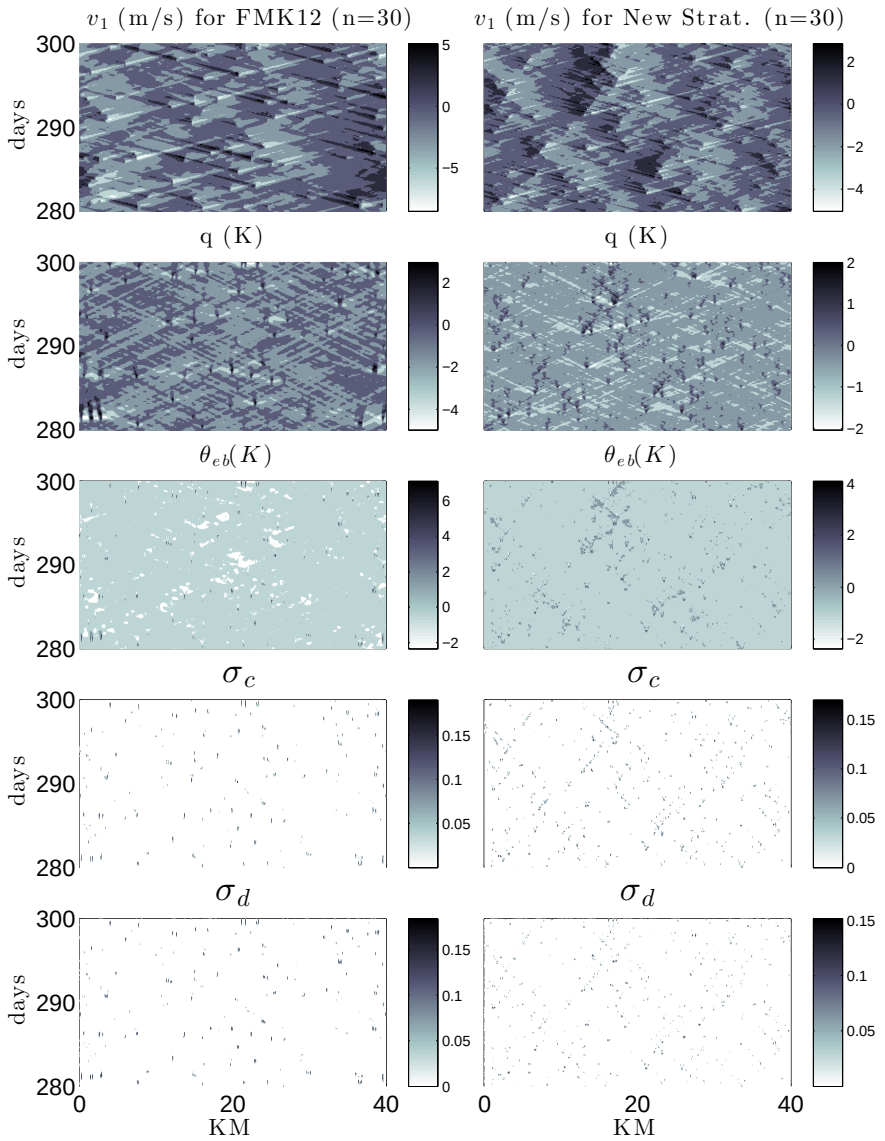

Fig. 5 x, t simulations for FMK12(left) and new stratiform heating closure (right). Both stochastic simulations use 900 cloud sites ($n = 30$). The parameters are as in Tables 1 and 2 and are the same as standard parameter regime of FMK12. For each of the simulations, we plot contours of five variables(top to bottom): first baroclinic velocity, moisture, ABL temperature, congestus and deep cloud fraction.

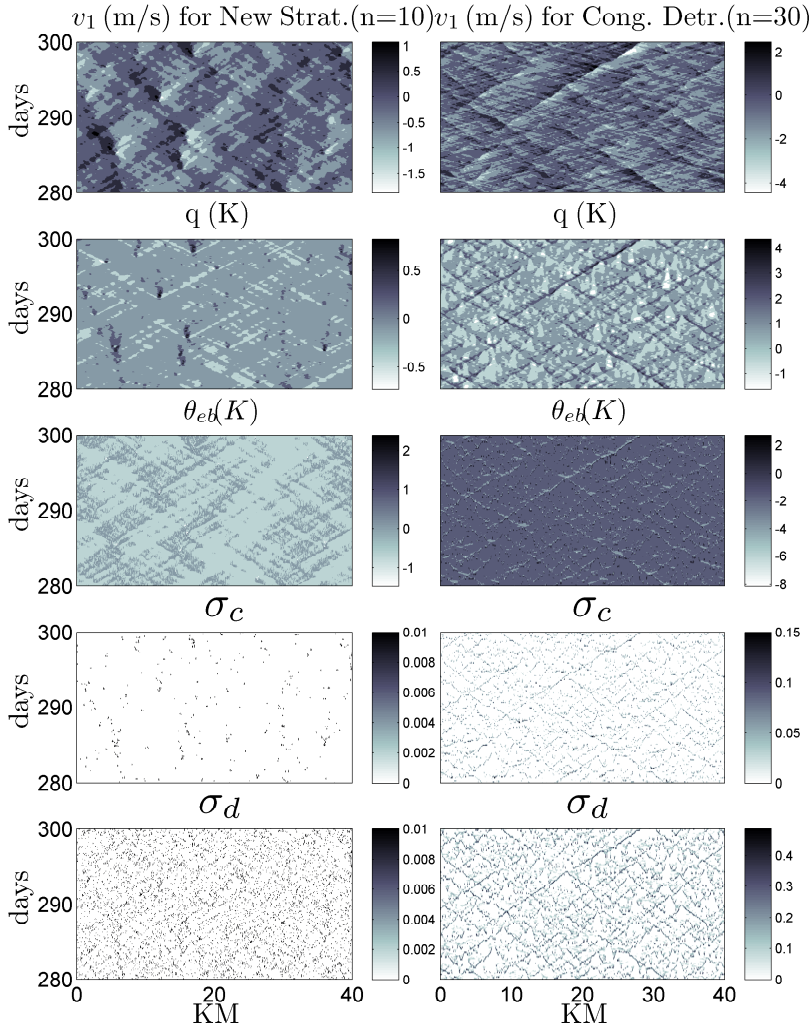

Fig. 6 x, t simulations with the new stratiform heating closure with a low number (n=10) of convective sites (left) and congestus detrainment regime with n=30 (right). For the new heating closure simulation, the parameters as in from Tables 1 and 2 and are the same as in the standard parameter regime of FMK12. Parameter modifications for the congestus detrainment regime are discussed in Section 3.3. For each of the simulations, we plot contours of five variables (top to bottom): first baroclinic velocity, moisture, ABL temperature, congestus and deep cloud fraction.

5.2 Warm pool background

This section presents the results of the stochastic and mean field $x-t$ simulations of the stochastic multicloud model with a 5K warm pool (2.1). The results are summarized in Table 3. The stochastic lag type stratiform closure greatly improves the coherence of variability and low number of convective cloud sites allows for even greater intermittency. The congestus detrainment mechanism allows for built up of moisture, which results in higher mean horizontal velocity of the walker circulation. In all cases, the stochastic models perform better than the deterministic counterpart.

The mean structure of the Walker circulation, obtained by a time average of 100 days of simulation, is discussed first. As was shown in FMK12, the deterministic multicloud model in a suboptimal parameter regime produces unreasonable mean circulation (top panels of Figures 7 and 8) driven by a sharp deep convective heating peak in the middle. The stochastic parameterization, introduced in FMK12, improves on this, with a more reasonable and stronger circulation as shown on the second panel of Figures 7 and 8. The high SST creates an enhanced convection region inside the warm pool resulting in a peak of deep convection in the center of the warm pool that drives the circulation. The pronounced peaks in deep convection, on the edges of the warm pool, are due to intermittent convectively coupled waves radiating away from the warm pool (going through a mature stage then losing strength and moisture as they move away from the warm pool). The introduction of the new stratiform heating closure does not change this tri-peak structure, as can be seen in the stochastic simulations with $n = 30$ in and $n = 10$ in second and third panels of Figure 8. The deterministic mean field limit simulation, shown on the 5th panel, has a suppressed tri-peak heating structure. This confirms the results of the homogenous SST simulation, that link the high increase in stochastic noise to an increase in the variability of deep convection. Congestus detrainment in the deterministic model fails to produce a physical result (see the second panel from bottom in Figures 7 and 8). On the other hand, congestus detrainment in the stochastic model allows for a built up of moisture in the center of the warm pool. This results in a single convective peak in the center that drives a circulation with highest horizontal velocity of any simulation in the paper (see bottom panels of Figures 7 and 8).

The left panels of Figure 9 present the $x-t$ simulations of FMK12 without the lag type stratiform closure, taken directly from FMK12. As pointed out in the FMK12, the characteristic features of the simulation are the persistent cloud decks confined to the warm pool area. Radiating away for the warm pool are convectively coupled waves, moving with a velocity of 14-18 m/s. The right panels of Figures 9 and the left panels of Figure 10 present the $x-t$ simulations of FMK12 with the lag type stratiform closure for $n = 30$ and $n = 10$, respectively. As was the case with the means, the deviations from the mean are very similar to the results of FMK12 with an increased coherence of the convective heating fields. The variability of the heating fields is summarized in Table 3. The simulation with the new stratiform heating closure and $n = 30$

Table 3 Mean circulation strength and variability of heating fields for the deterministic, stochastic and deterministic mean field limit simulations with 5K SST background.

Regime	model	n	warm pool max (U, W)	$std(H_d)$	std(H_c)
FMK12	determenistic	-	$(3m/s, 4cm/s)$	0.97 K/Day	0.14 K/Day
FMK12	stochastic	n=30^2	$(10m/s, 3cm/s)$	1.67 K/Day	1.89 K/Day
New heating closure	stochastic	n=30^2	$(9m/s, 3cm/s)$	1.58 K/Day	4.08 K/Day
New heating closure	stochastic	n=10^2	$(9m/s, 2cm/s)$	6.24 K/Day	8.43 K/Day
New heating closure	DMFLE	-	$(10m/s, 2cm/s)$	1.36 K/Day	16.97 K/Day
Congestus Detr.	determenistic	-	$(7m/s, 2cm/s)$	1.04 K/Day	0.34 K/Day
Congestus Detr.	stochastic	n=30^2	$(14m/s, 2cm/s)$	1.44 K/Day	17.04 K/Day

has lower variability than the simulation from FMK12 with the same number of cloud sites. However, in the simulation with new lag closure and $n = 10$, the maximum variance of the deep convective field is almost 3 times as large as the one recorded in the FMK12 simulation. Thus, we have significantly improved the variability of the warm pool, while maintaining the coherence of the wave structures. Interestingly, the DMFLE simulations have the lowest variability of deep convection but highest variability of congestus heating.

The stochastic simulations with congestus detrainment mechanism are shown on the right panels of Figure 10. The solution is characterized by a relatively high variability of congestus heating. Of high interest are the 3 m/s envelope structures outside of the warm pool, which are associated with the congestus clouds and the intermittent but large deep convective events. While the overall variability of the deep convective heating field is lower compared to the stochastic multicloud models without congestus detrainment, the model still outperforms its deterministic counterpart.

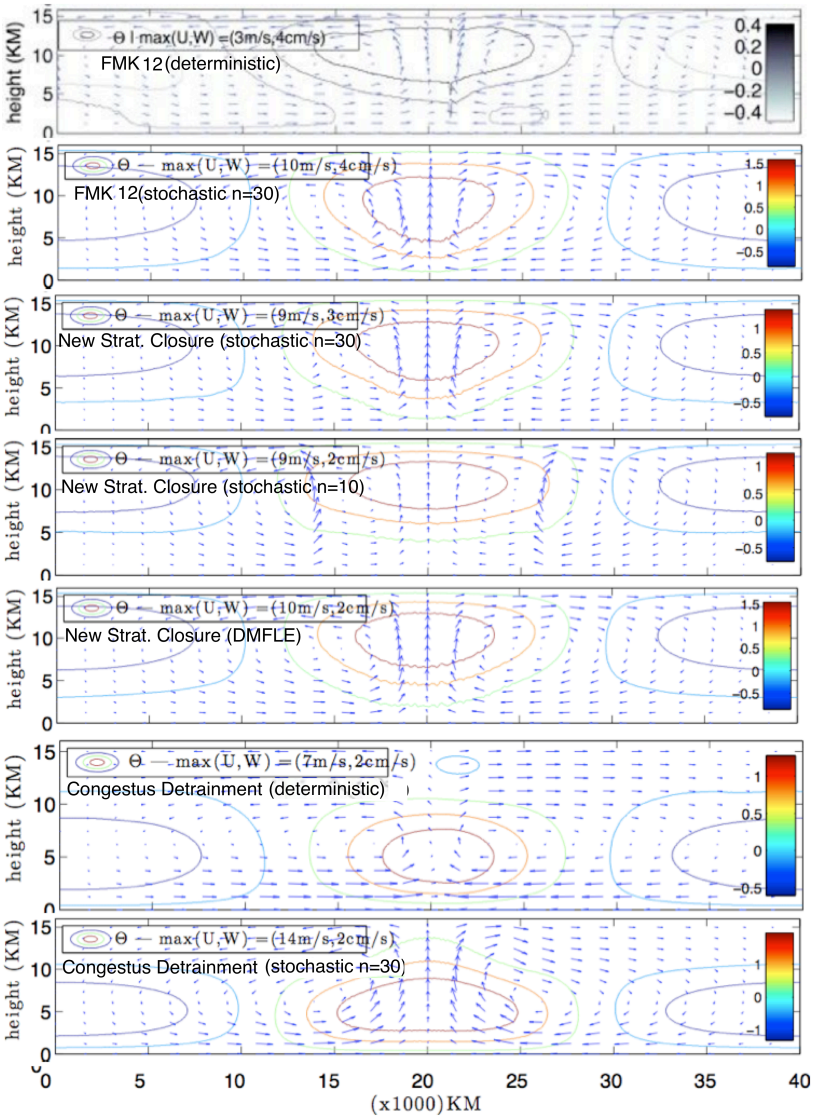

Fig. 7 Vertical structure of Walker simulation computed from 100 days time average of the multicloud model simulations (top to bottom): deterministic FMK12, stochastic FMK12 n=30, stochastic new stratiform closure (n=30),stochastic new stratiform closure (n=10), DMFL stratiform closure, deterministic congestus detrainment and stochastic congestus detrainment simulations.

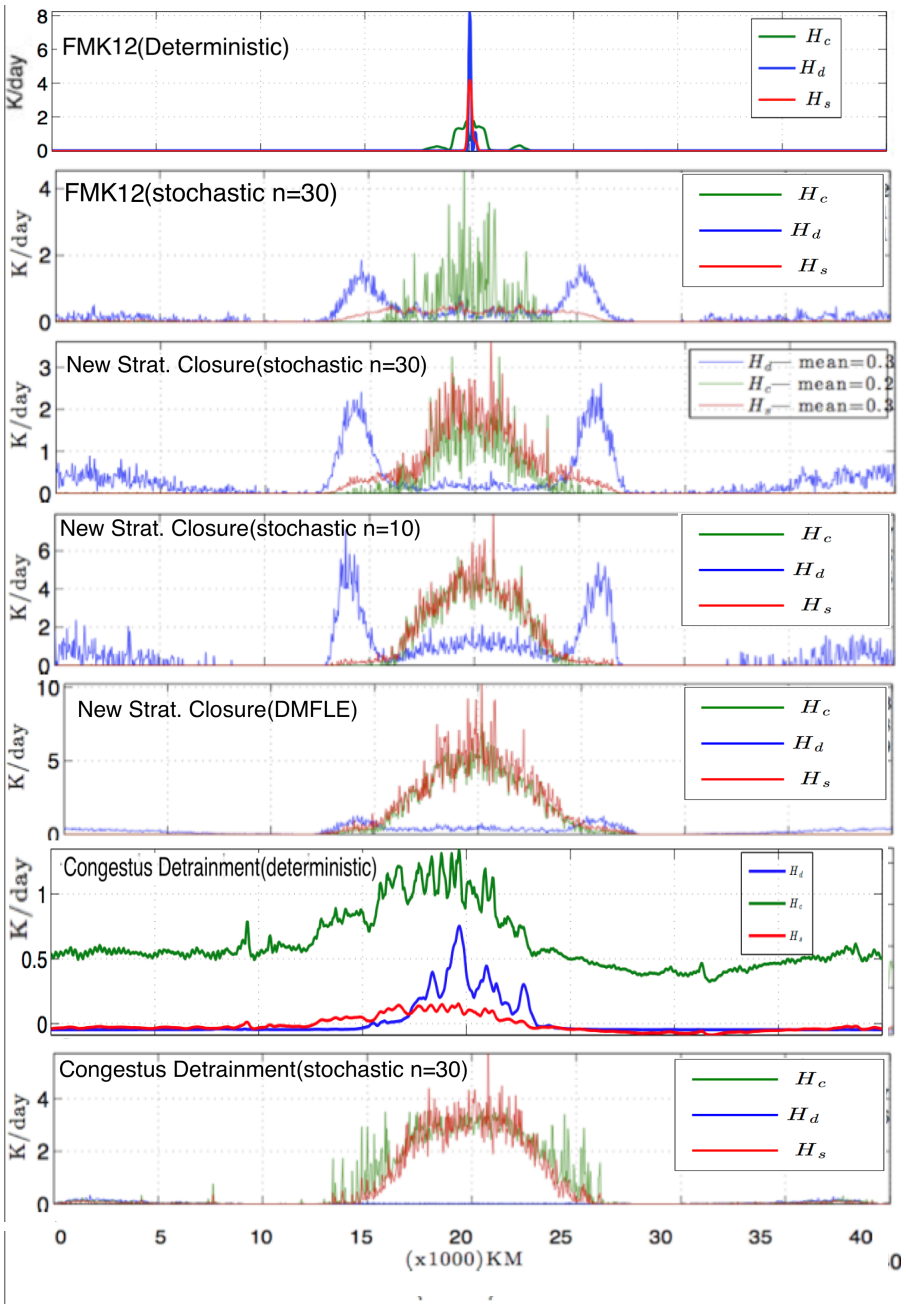

Fig. 8 Same as fig. 7 but for convective heating rates.

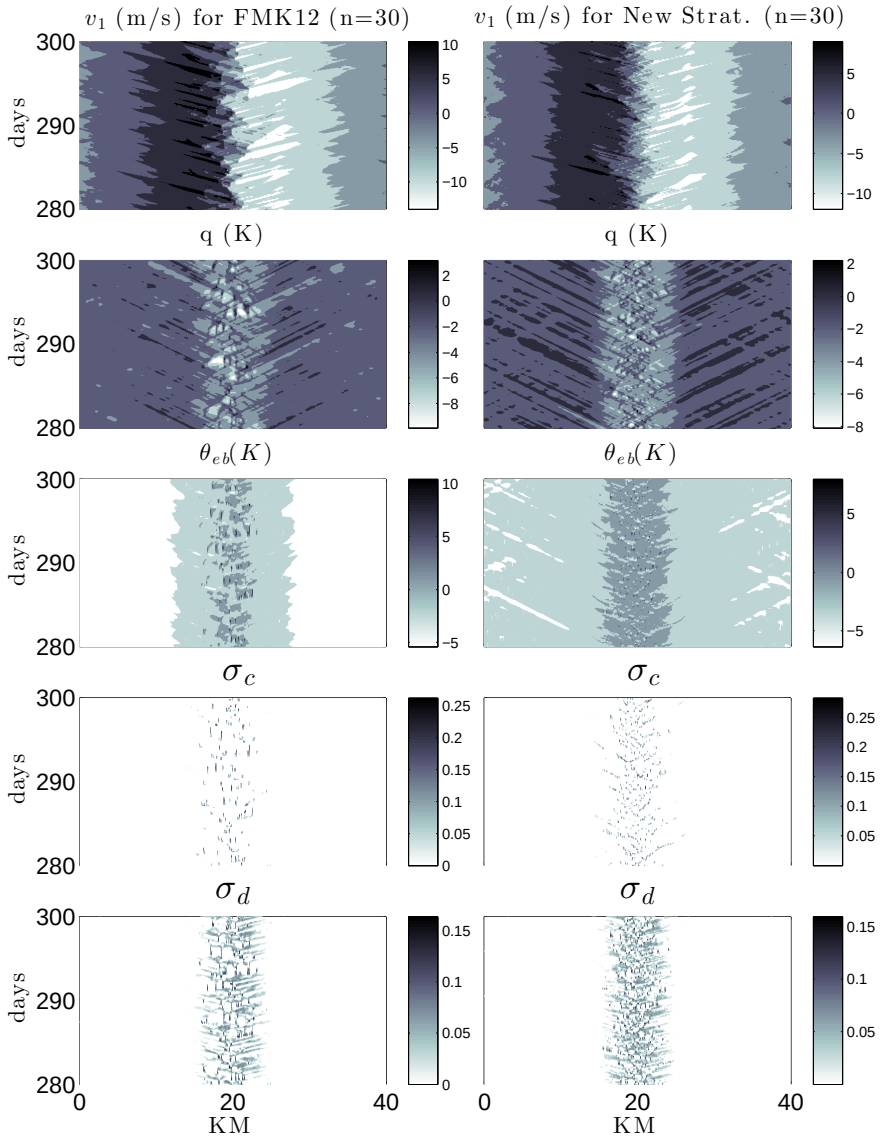

Fig. 9 Same as Figure 5 but for the 5K SST warm pool.

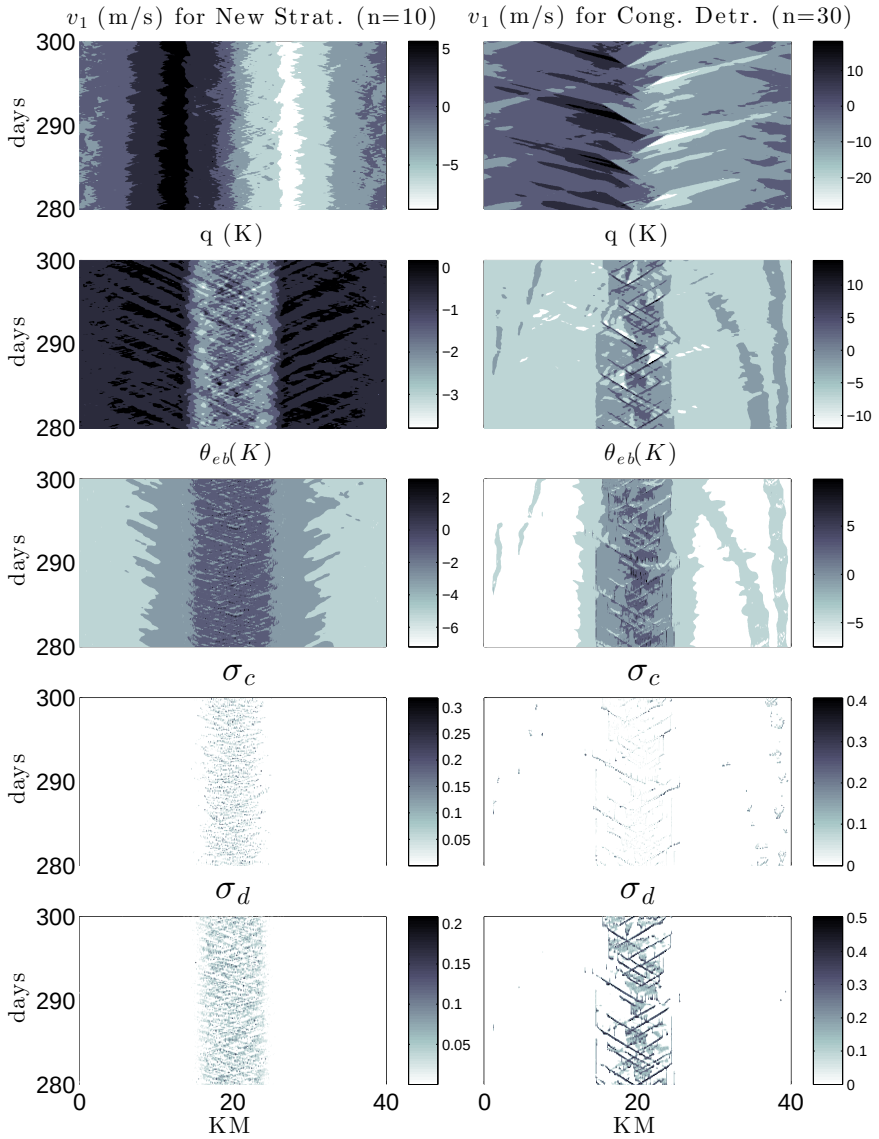

Fig. 10 Same as Figure 6 but for the 5K SST warm pool.

5.3 Statistical analysis and comparison with observations

This section presents analysis of statistics of precipitation and water vapor for the stochastic multicloud model results presented in the previous section. We consider three regimes: FMK12 parameter regime ($n = 30$), FMK12 with lag type stratiform heating closure ($n = 10$) and the newly developed congestus detrainment ($n = 30$). The results are compared to observations and theoretical studies.

The motivation of this section comes form observational studies in [33, 12], where the authors concentrate on time series analysis of water vapor and precipitation from radiosonde and gauge data at the Nauru site of the Atmospheric Radiation Measurement (ARM) mission. To produce similar statistical analysis, the spatially extended simulations of the stochastic multicloud model with homogeneous SST background are sampled at fixed sites. The results from individual "observation sites" are connected to produce a single time series. A spacing of 2,000 km, between two adjacent sites, is chosen to insure the lack of significant correlations in the resulting time series. All the simulations are run for 300 days using the methods described in the beginning of the section. The first 200 days of the simulation are discarded while the last 100 days are sampled to produce the 2000 day time series. The sampling rate of one hour is chosen, which is of the order of the sampling rate commonly found in radiosonde [12] and satellite observations.

The auto correlation function for deep convective heating and moisture is shown on the left panels of Figure 11 for the three regimes discussed above. This figure can be directly compared to Fig 1. of [13]. Similarly to [12,13], the autocorrelation of deep convection is short compared to the autocorrelation of moisture. The results for the simulations with lag type stratiform closure show appreciably lower auto-correlation of deep convection compared to the simulations with FMK12 closure. The model with congestus detrainment has the lowest autocorrelation of deep precipitation, as could be surmised from observing the highly intermittent and short deep convective heating spikes in our previous results.

The second statistical measure considered here is the distribution of the precipitation events. Here we define precipitation events in the manner analogous to [44,47,46]. The precipitation event is defined as an uninterrupted sequence of time steps with deep or stratiform convective cloud fraction greater than RCE value. The first step in this sequence must be positive deep cloud fraction anomaly. The simulations for all three regimes are given in right panels of Figure 11, where the frequency of occurence is plotted as a function of the total mm of precipitation per event (which is obtained by integrating the precipitation rate over the life time of the precipitation event); we use the fact that approximately 4 mm of rain corresponds roughly to heating a 1 m^2-atmospheric column of air, under normal atmospheric conditions, by 1 K. The power-law decay of precipitation events observed in all three spatially extended simulations is in quantitative agreement with observations. The occurrence frequency, in the right panels of Fig. 11, for precipitation events

greater than 1 mm, falls approximately by 2 factors of 10 over a range of about 1 factor of 10 in total precipitation. Similar power-law is found in the observational studies of [44,47] and [48] but for heavier precipitation events, of size 10mm or greater. The power law for the smaller events in the present simulations, with total size of 1mm or less, are relatively flat consistent with the ARM observations shown in [44,47,52].

The correct reproduction of the above features is contingent upon site specific sampling of the spatially extended multicloud model. A time series taken from single column stochastic multicloud model simulations yields similar autocorrelation results but fails to correctly reproduce the precipitation events distribution. This points to the importance of gravity waves and large scale moisture convergence in the model. The overall results produced here, through the stochastic multicloud model, are similar to those in [52], which used a simple stochastic Markov-jump process to model for the transition to deep convection. In their study, the authors found that the stochastic "external" forcing in the column model to be crucial for correct reproduction of the large precipitation statistics. The results here show that the stochastic multicloud model produces such forcing automatically through consistent nonlinear dynamics.

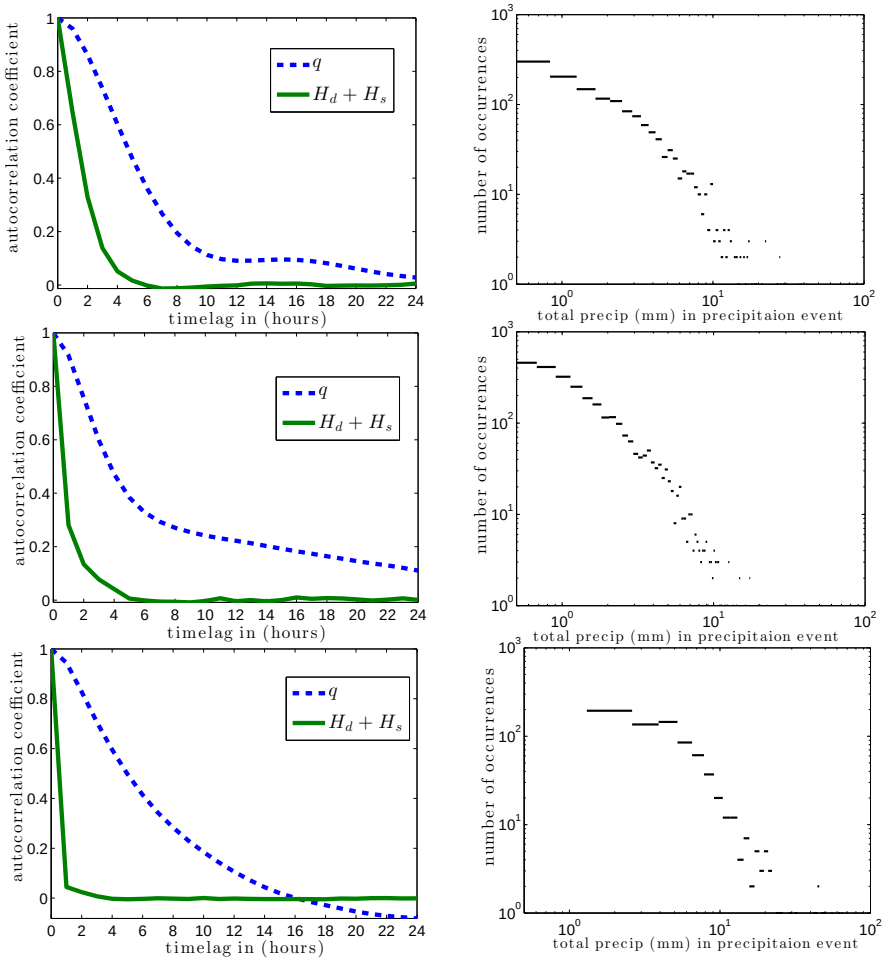

Fig. 11 Autocorrelation (left) and distribution of the precipitation events (right) for stochastic multicloud model in (top to bottom) FMK12, FMK with lag type stratiform closure and congestus detrainment. Compare the left panels to the observational data in Fig 1 of [13] and theoretical study in Fig 1 of [52]. Compare the left panels to the power laws seen in Fig 6b of [44], in Fig 1 of [48], in Figs. 2 and 3a of [46] and in Fig. 4 of [52]

6 Conclusions

Here a modified version of the stochastic multicloud model (KBM10,FMK12) is used to study horizontally homogeneous one column model dynamics and flows above the equator without rotation effects. The model is based on a coarse grained Markov chain lattice model where each lattice site takes discrete values from 0 to 3 according to whether the site is clear sky or occupied by a congestus, deep or stratiform cloud. The convective elements of the model interact with each other and with the large scale environmental variables through CAPE and middle troposphere dryness.

This paper improves upon the results of FMK12 by introducing a new lag-type ODE stratiform heating closure, which enhances the coherence of the convectively coupled waves in the model. This additional coherence allows us to consider parameter regimes with higher amounts of stochastic noise. The result is a Walker type circulation with a variability that exceeds the results of FMK12. Secondly, a congestus detrainment moistening mechanism is added to the multicloud framework. In the stochastic simulations, congestus detrainment mechanism allows for an effective moisture preconditioning. In addition, the deterministic mean field limit equations (DMFLE) for stochastic multicloud model are derived as a bridge between the deterministic and the stochastic multicloud parameterizations.

Building on the work of FMK12, it is found here that the stochastic lag-type stratiform closure greatly improves the synchronization of the stratiform heating and stratiform cloud fraction in the one column simulations (Section 4). In the spatially extended system, the new closure further improves the coherence of stratiform and congestus heating fields. This additional coherence allows us to consider parameter regimes with higher amounts of stochastic noise. This in particular results in a Walker type circulation with an increased variability of the fluctuations about the mean that exceeds the results of FMK12.

The congestus detrainment moistening mechanism provides a powerful way of increasing the overall strength and the variability of the warm pool simulations. It is a regime dominated by persistent congestus episodes which are followed by rare but strong deep convective events. This regime features a Walker type circulation with a large low-level mean zonal velocity, which is associated with a congestus preconditioning driven deep precipitation peak in the center.

A comparison of site specific observations to nature is carried out in Sec 5.3. It shows that stochastic multicloud model captures qualitatively two local statistical features of the observations. First, auto-correlation functions of moisture and precipitation have long and short autocorrelation times, respectively. Second, the power laws in the precipitation event size distribution follow the 2 to 1 ratio observed for large precipitation events. The latter is only possible when spatially extended (but not column) simulations are considered. This points to the importance of gravity waves and large scale moisture convergence. This conclusion was also emphasized in [52], where the authors use stochastic "external" forcing in the column setup to mimic these impor-

tant effects. Furthermore, we note that the statistics obtained with improved stochastic multicloud model, both with lag type stratiform closure and congestus detrainment mechanism, are in a better agreement compared to FMK12. This clearly demonstrates and confirms the intuition about improvements introduced here.

As already stated, the deterministic mean field limit equations allow us to separate the roles of the stochastic and deterministic chaos in the system and provide a connection to the deterministic multicloud model. The one column simulations of Section 4, provide three distinct examples of the nature of chaotic dynamics in the stochastic parameterizations. The FMK12 regime is characterized by inherently stable deterministic oscillations with stochastic noise providing deviations and adding complexity to the behavior. The stochastic simulations with the new stratiform heating closure contain both stochastic and deterministic chaos. The congestus detrainment moistening regime has chaotic behavior built into the mean field model. Thus, in some regimes, the DMFLE parameterization is capable of producing chaotic behavior. In these regimes, the stochastic parameterization could be computationally cheaper to evolve, given the stiff nature of the DMFLE. Furthermore, under simplifying assumptions, the DMFLE can be connected to deterministic multicloud model, to provide a link between the stochastic and deterministic multicloud parameterizations. Of particular importance, we note that the statistics obtained with improved stochastic multicloud model, with both lag stratiform and congestus detrainment, are in a better agreement with observation while those associated with the lag-stratiform closure are intermediate between the old FMK12 model the fully improved model. This clearly demonstrates and confirms the intuition about the sequencing of the improvements introduced here.

In general, the stochastic parameterization improves on its deterministic counterpart in terms of magnitude and structure of the variability. Coherent intermittent wave structures characterize the solutions of the stochastic multicloud model. Depending on the regime, this intermittency can come from the stochastic "noise" of the model or from the intrinsically stiff nature of the parameterization (that is from the mean field equations). The amplitude of the variability (as well as its intermittency) can be increased by considering regimes with fewer convective elements, which amounts to increasing the stochastic noise.

Acknowledgements The research of B.K. is supported in part by the Natural Sciences and Engineering Research Council of Canada. The research of A. J. M. is partially supported by National Science Foundation grants DMS-0456713 and DMS-1025468 and by the office of Naval Research grants ONR DRI N0014-10-1-0554 and N00014-11-1-0306. Y. F. is a postdoctoral fellow supported through A.J.Ms above NSF and ONR grants.

A Derivation of approximations for congestus and deep heating

Here derive approximations for congestus and deep heating. We begin by considering a regime where the dependency of the cloud fractions on CAPE (and low level CAPE) is suppressed.

In this scenario, the cloud fraction transition rates are determined by fluctuations in dryness alone. This is accomplished by replacing CAPE and low level CAPE dependency in the transition rates by the RCE value of CAPE.

$$\hat{R}_{01} = \frac{1}{\tau_{01}} \Gamma(\bar{C}) \Gamma(D) \tag{36}$$

$$\hat{R}_{12} = \frac{1}{\tau_{12}} \Gamma(\bar{C})(1 - \Gamma(D)) \tag{37}$$

$$\hat{R}_{02} = \frac{1}{\tau_{02}} \Gamma(\bar{C})(1 - \Gamma(D)) \tag{38}$$

$$\hat{R}_{20} = \frac{1}{\tau_{20}} (1 - \Gamma(\bar{C})) \tag{39}$$

The hats are used to distinguish the modified rates used here for the purpose of comparison from the actual transition rates listed in Table 2. Here, $\bar{C}$ is the RCE value of scaled CAPE, and scaled low level CAPE, in (19) and (18), respectively. The two quantities are equal at RCE. As before, D is the scaled dryness of the troposphere (20).
First, we consider the congestus heating equation for, the stochastic multicloud model.

$$H_c = \sigma_c \frac{\alpha_c \bar{\alpha}}{H_m} \sqrt{CAPE_l^+}. \tag{40}$$

At this point, we can take a derivative of the above expression to obtain

$$\dot{H}_c = \dot{\sigma}_c \frac{\alpha_c \bar{\alpha}}{H_m} \sqrt{CAPE_l^+} + \frac{\bar{\alpha} \alpha_c}{2 H_m} \sigma_c ({CAPE_l}^+)^{-1/2} \dot{CAPE_l}. \tag{41}$$

We assume that variations in $CAPE_l$ are small relative to the amount of $CAPE_l$, as it would be the case near equilibrium. This allows us to concentrate on the first term of the expression above. Using (30), we write

$$\dot{H}_c \approx \frac{\alpha_c \bar{\alpha}}{H_m} (\sigma_{cs} \hat{R}_{01} - \sigma_c (\hat{R}_{10} + \hat{R}_{12})) \sqrt{CAPE_l^+}. \tag{42}$$

With the simplified transition rates (36) and (37) and using the definitions of the rate R_{10} from Table 2, we can rewrite Eq. 42 as

$$\dot{H}_c \approx \frac{\alpha_c \bar{\alpha}}{H_m} \left[\left(\sigma_{cs} \frac{\Gamma(\bar{C})}{\tau_{01}} + \sigma_c \frac{\tau_{01} \Gamma(\bar{C}) - \tau_{12}}{\tau_{10} \tau_{12}} \right) \Gamma(D) - \sigma_c \frac{\Gamma(\bar{C})}{\tau_{12}} \right] \sqrt{CAPE_l^+} \tag{43}$$

and from (40), we get

$$\dot{H}_c \approx \frac{\Gamma(\bar{C})}{\tau_{12}} \left(\frac{\alpha_c \bar{\alpha} \tau_{12}}{H_m \Gamma(\bar{C})} \left(\sigma_{cs} \frac{\Gamma(\bar{C})}{\tau_{01}} + \sigma_c \frac{\tau_{01} \Gamma(\bar{C}) - \tau_{12}}{\tau_{10} \tau_{12}} \right) \Gamma(D) \sqrt{CAPE_l^+} - H_c \right). \tag{44}$$

Furthermore, since $\sigma_c \ll \sigma_{cs} \approx 1$, we arrive at

$$\dot{H}_c \approx \frac{\Gamma(\bar{C})}{\tau_{12}} \left(\frac{\tau_{12} \alpha_c \bar{\alpha}}{\tau_{01} H_m} \Gamma(D) \sqrt{CAPE_l^+} - H_c \right). \tag{45}$$

In fact, we can rewrite the equation for the evolution of congestus heating in a simpler and more familiar form,

$$\dot{H}_c \approx \frac{1}{\tau_c^{MFL}}(\alpha_c^{MFL}\Gamma(D)\sqrt{CAPE_l^+} - H_c) \tag{46}$$

where

$$\tau_c^{MFL} = \frac{\tau_{12}}{\Gamma(\bar{C})}\alpha_c^{MFL} = \alpha_c\frac{\tau_{12}\bar{\alpha}}{\tau_{01}H_m}. \tag{47}$$

In order to derive equation for approximate deep convective heating. We consider equation Eq. 31 and make an assumption that the adjustment of deep convective cloud fraction is instantaneous. This yields approximation equation for the deep convective cloud fraction

$$\sigma_d \approx \frac{\sigma_{cs}\hat{R}_{02} + \sigma_c\hat{R}_{12}}{(\hat{R}_{20} + \hat{R}_{23})}. \tag{48}$$

Using the simplified transition rates (37 - 39) and constant transition rate R_{23} from Table 2, this approximation takes form:

$$\sigma_d \approx \left[\frac{(\frac{\sigma_{cs}}{\tau_{02}} + \frac{\sigma_c}{\tau_{12}})\Gamma(\bar{C})}{(\frac{1}{\tau_{23}} + \frac{1-\Gamma(\bar{C})}{\tau_{20}})}\right]\Big(1 - \Gamma(D)\Big) \tag{49}$$

Again, since $\sigma_c \ll \sigma_{cs} \approx 1$, we write the last expression as

$$\sigma_d \approx \left[\frac{\tau_{23}\tau_{20}\Gamma(\bar{C})}{\tau_{02}(\tau_{20} + \tau_{23}(1 - \Gamma(\bar{C}))}\right]\left(1 - \Gamma(D)\right). \tag{50}$$

Under the above simplifying assumptions, using (23), deep convective heating is given approximately by

$$H_d \approx \left[\frac{\tau_{23}\tau_{20}\Gamma(\bar{C})}{\tau_{02}(\tau_{20} + \tau_{23}(1 - \Gamma(\bar{C}))}\right]\left(1-\Gamma(D)\right)\left[\bar{Q}+\frac{1}{\tau_{conv}^0\bar{\sigma_d}}(a_1\theta_{eb}+a_2q-a_0(\theta_1+\gamma_2\theta_2))\right]^+. \tag{51}$$

References

1. Arakawa, A., Schubert, W.H.: Interaction of a cumulus cloud ensemble with the large-scale environment, Part I. J. Atmos. Sci. **31**, 674–701 (1974)
2. Betts, A.K., Miller, M.J.: A new convective adjustment scheme. Part II: Single column tests using GATE wave, BOMEX, ATEX and Arctic air-mass data sets. Quarterly Journal of the Royal Meteorological Society **112**(473), 693–709 (1986)
3. Buizza, R., Miller, M., Palmer, T.N.: Stochastic representation of model uncertainties in the ECMWF Ensemble Prediction System. Quarterly Journal of the Royal Meteorological Society **125**, 2887–2908 (1999)
4. ECMWF: Proceedings ECMWF/CLIVAR Workshop on Simulation and Prediction of Intraseasonal variability with Emphasis on the MJO pp. 3–6 November (2003)
5. Frenkel, Y., Majda, A.J., Khouider, B.: Using the stochastic multicloud model to improve tropical convective parameterization: A paradigm example. J. Atmos. Sci. **69**(3), 1080–1105 (2012)
6. Gillespie, D.T.: An exact method for numerically simulating the stochastic coalescence process in a cloud. J. Atmos. Sci. **32**, 1977–1989 (1975)
7. Grabowski, W.W.: Coupling cloud processes with the large-scale dynamics using the cloud-resolving convection parameterization. J. Atmos. Sci. **58**(9), 978–997 (2001)
8. Grabowski, W.W.: An improved framework for superparameterization. J. Atmos. Sci. **61**(15), 1940–1952 (2004)

9. Grabowski, W.W., Smolarkiewicz, P.K.: CRCP: A Cloud Resolving Convection Parameterization for modeling the tropical convecting atmosphere. Physica D Nonlinear Phenomena **133**, 171–178 (1999)
10. Han, Y., Khouider, B.: Convectively coupled waves in a sheared environment. J. Atmos. Sci. **67**, 2913–2942 (2010)
11. Hendon, H.H., Liebmann, B.: Organization of convection within the Madden–Julian oscillation. **99**, 8073–8084 (1994)
12. Holloway, C.E., Neelin, J.D.: Moisture Vertical Structure, Column Water Vapor, and Tropical Deep Convection. Journal of Atmospheric Sciences **66**, 1665 (2009)
13. Holloway, C.E., Neelin, J.D.: Temporal Relations of Column Water Vapor and Tropical Precipitation. Journal of Atmospheric Sciences **67**, 1091–1105 (2010)
14. Horenko, I.: Nonstationarity in multifactor models of discrete jump processes, memory and application to cloud modeling. J. Atmos. Sci. **68**, 1493–1506 (2011)
15. Johnson, R.H., Rickenbach, T.M., Rutledge, S.A., Ciesielski, P.E., Schubert, W.H.: Trimodal characteristics of tropical convection. Journal of Climate **12**(8), 2397–2418 (1999)
16. Kain, J.S., Fritsch, J.M.: A one-dimensional entraining/detraining plume model and its application in convective parameterization. J. Atmos. Sci. **47** (1990)
17. Katsoulakis, M.A., Majda, A.J., Vlachos, D.G.: Coarse-grained stochastic processes for microscopic lattice systems. Proceedings of the National Academy of Sciences of the United States of America **100**(3), 782–787 (2003)
18. Katsoulakis, M.A., Majda, A.J., Vlachos, D.G.: Coarse-grained stochastic processes and monte carlo simulations in lattice systems. Journal of Computational Physics **186**(1), 250 – 278 (2003b)
19. Khouider, B., Biello, j., Majda, A.J.: A stochastic multicloud model for tropical convection. Comm. Math. Sci. **8**(1), 187–216 (2010)
20. Khouider, B., Majda, A.J.: A non oscillatory balanced scheme for an idealized tropical climate model; Part I: Algorithm and validation. Theoretical and Computational Fluid Dyn. **19**, 331–354 (2005)
21. Khouider, B., Majda, A.J.: A non oscillatory balanced scheme for an idealized tropical climate model; Part II: Nonlinear coupling and moisture effects. Theoretical and Computational Fluid Dyn. **19**, 355–375 (2005)
22. Khouider, B., Majda, A.J.: Multicloud convective parametrizations with crude vertical structure. Theor. Comp. Fluid Dyn. **20**, 351–375 (2006)
23. Khouider, B., Majda, A.J.: A simple multicloud parametrization for convectively coupled tropical waves. Part I: Linear analysis. J. Atmos. Sci. **63**, 1308–1323 (2006)
24. Khouider, B., Majda, A.J.: A simple multicloud parametrization for convectively coupled tropical waves. Part II: Nonlinear simulations. J. Atmos. Sci. **64**, 381–400 (2007)
25. Khouider, B., Majda, A.J.: Equatorial convectively coupled waves in a simple multicloud model. J. Atmos. Sci. **65**, 3376–3397 (2008)
26. Khouider, B., Majda, A.J.: Multicloud models for organized tropical convection: Enhanced congestus heating. J. Atmos. Sci. **65**, 897–914 (2008)
27. Khouider, B., Majda, A.J., Katsoulakis, M.A.: Coarse-grained stochastic models for tropical convection and climate. Proceedings of the National Academy of Science **100**, 11,941–11,946 (2003)
28. Khouider, B., St-Cyr, A., Majda, A.J., Tribbia, J.: MJO and convectively coupled waves in a coarse resolution GCM with a simple multicloud parametrization. J. Atmos. Sci. **68**, 240–264 (2010)
29. Kuo, H.L.: Further studies of the parameterization of the influence of cumulus convection on large-scale flow. J. Atmos. Sci. **31**, 1232–1240 (1974)
30. Lau, W.K.M., Waliser, D.E.: Intraseasonal Variability in the Atmosphere-Ocean Climate System. Springer-Verlag (2005)
31. Lin, J., Neelin, J.D.: Toward stochastic deep convective parameterization in general circulation models. **30**(4), 1162 (2003)
32. Lin, J.L., Kiladis, G.N., Mapes, B.E., Weickmann, K.M., Sperber, K.R., Lin, W., Wheeler, M.C., Schubert, S.D., Del Genio, A., Donner, L.J., Emori, S., Gueremy, J.F., Hourdin, F., Rasch, P.J., Roeckner, E., Scinocca, J.F.: Tropical intraseasonal variability in 14 IPCC AR4 climate models. Part I: Convective signals. Journal of Climate **19**(12), 2665–2690 (2006)

33. Lintner, B.R., Holloway, C.E., Neelin, J.D.: Column Water Vapor Statistics and Their Relationship to Deep Convection, Vertical and Horizontal Circulation, and Moisture Structure at Nauru. Journal of Climate **24**, 5454–5466 (2011)
34. Majda, A.J.: Multiscale models with moisture and systematic strategies for superparameterization. J. Atmos. Sci. **64**(7), 2726–2734 (2007)
35. Majda, A.J., Franzke, C., Khouider, B.: An applied mathematics perspective on stochastic modelling for climate. Philosophical Transactions of the Royal Society A: Mathematical, Physical and Engineering Sciences **366**(1875), 2427–2453 (2008)
36. Majda, A.J., Khouider, B.: Stochastic and mesoscopic models for tropical convection. Proceedings of the National Academy of Science **99**, 1123–1128 (2002)
37. Majda, A.J., Stechmann, S., Khouider, B.: MaddenJulian Oscillation analog and intraseasonal variability in a multicloud model above the equator. Proceedings of the National Academy of Science **104**, 9919–9924 (2007)
38. Majda, A.J., Stechmann, S.N.: Stochastic models for convective momentum transport. Proceedings of the National Academy of Sciences **105**(46), 17,614–17,619 (2008)
39. Manabe, S., Smagorinsky, J., Strickler, R.F.: Simulated climatology of a general circulation model with a hydrologic cycle1. Monthly Weather Review **93**(12), 769–798 (1965)
40. Mapes, B.E.: Convective inhibition, subgrid-scale triggering energy, and stratiform instability in a toy tropical wave model. J. Atmos. Sci. **57**(10), 1515–1535 (2000)
41. Moncrieff, M., Shapiro, M., Slingo, J., Molteni, F.: Collaborative research at the intersection of weather and climate. WMO Bulletin **56**, 204–211 (2007)
42. Moncrieff, M.W., Klinker, E.: Organized convective systems in the tropical western Pacific as a process in general circulation models: A TOGA COARE case-study. Quarterly Journal of the Royal Meteorological Society **123**, 805–827 (1997)
43. Nakazawa, T.: Tropical super clusters within intraseasonal variation over the western pacific. J. Meteorol. Soc. Japan **66**, 823–839 (1974)
44. Neelin, J.D., Peters, O., Lin, J.W.B., Hales, K., Holloway, C.E.: Rethinking convective quasi-equilibrium: observational constraints for stochastic convective schemes in climate models. Royal Society of London Philosophical Transactions Series A **366**, 2579–2602 (2008)
45. Palmer, T.N.: A nonlinear dynamical perspective on model error: A proposal for nonlocal stochastic-dynamic parametrization in weather and climate prediction models. Quarterly Journal of the Royal Meteorological Society **127**, 279–304 (2001)
46. Peters, O., Deluca, A., Corral, A., Neelin, J.D., Holloway, C.E.: Universality of rain event size distributions. Journal of Statistical Mechanics: Theory and Experiment **11**, 30 (2010)
47. Peters, O., Neelin, J.D.: Atmospheric Convection as a Continuous Phase Transition:. Further Evidence. International Journal of Modern Physics B **23**, 5453–5465 (2009)
48. Peters, O., Neelin, J.D., Nesbitt, S.: Mesoscale convective systems and critical clusters. AGU Spring Meeting Abstracts p. A5 (2009)
49. Randall, D., Khairoutdinov, M., Arakawa, A., Grabowski, W.: Breaking the cloud parameterization deadlock. Bulletin of the American Meteorological Society **84**(11), 1547–1564 (2003)
50. Scinocca, J.F., McFarlane, N.A.: The variability of modeled tropical precipitation. J. Atmos. Sci. **61**, 1993–2015 (2004)
51. Slingo, J.M., Sperber, K.R., Boyle, J.S., Ceron, J., Dix, M., Dugas, B., Ebisuzaki, W., Fyfe, J., Gregory, D., Gueremy, J., Hack, J., Harzallah, A., Inness, P., Kitoh, A., Lau, W., McAvaney, B., Madden, R., Matthews, A., Palmer, T.N., Parkas, C., Randall, D., Renno, N.: Intraseasonal oscillations in 15 atmospheric general circulation models: results from an AMIP diagnostic subproject. Climate Dynamics **12**, 325–357 (1996)
52. Stechmann, S.N., Neelin, J.D.: A stochastic model for the transition to strong convection. J. Atmos. Sci. **68**, 2955–2970 (2011)
53. Takayabu, Y.N.: Large-scale cloud disturbances associated with equatorial waves. part I: Spectral features of the cloud disturbances. J. Meteor. Soc. Japan **72**, 433–448 (1994)
54. Wheeler, M., Kiladis, G.N.: Convectively coupled equatorial waves: Analysis of clouds and temperature in the wavenumber-frequency domain. J. Atmos. Sci. **56**(3), 374–399 (1999)

55. Xing, Y., Majda, A.J., Grabowski, W.W.: New efficient sparse spacetime algorithms for superparameterization on mesoscales. Monthly Weather Review **137**(12), 4307–4324 (2009)
56. Zhang, C.: Madden–Julian oscillation. Reviews of Geophysics **43**, RG2003 (2005)
57. Zhang, G.J., McFarlane, N.A.: Sensitivity of climate simulations to the parameterization of cumulus convection in the Canadian Climate Centre General Circulation Model. Atmos.-Ocean **33**, 406–446 (1995)